Research Paper

GEOSPHERE

GEOSPHERE, v. 16, no. 5

https://doi.org/10.1130/GES01535.1

17 figures; 1 table; 1 set of supplemental files

CORRESPONDENCE: ann.timmermans@unb.ca

CITATION: Timmermans, A.C., Cousens, B.L., and Henry, C.D., 2020, Geochemical study of Cenozoic mafic volcanism in the west-central Great Basin, western Nevada, and the Ancestral Cascades Arc, California: Geosphere, v. 16, no. 5, p. 1179–1207, https://doi.org/10.1130/GES01535.1.

Science Editor: Shanaka de Silva
Associate Editor: Eric H. Christiansen

Received 10 March 2017
Revision received 19 October 2019
Accepted 1 May 2020

Published online 10 July 2020

Geochemical study of Cenozoic mafic volcanism in the west-central Great Basin, western Nevada, and the Ancestral Cascades Arc, California

Ann C. Timmermans[1,*], Brian L. Cousens[1], and Christopher D. Henry[2]

[1]Ottawa-Carleton Geoscience Centre and Isotope Geology and Geochronology Research Facility, Department of Earth Sciences, Carleton University, 1125 Colonel By Drive, Ottawa, Ontario, Canada, K1S 5B6
[2]Nevada Bureau of Mines and Geology, University of Nevada Reno, Reno, Nevada 89557, USA

ABSTRACT

Processes linked to shallow subduction, slab rollback, and extension are recorded in the whole-rock major-, trace-element, and Sr, Nd, and Pb isotopic compositions of mafic magmatic rocks in both time and space over southwestern United States. Eocene to Mio-Pliocene volcanic rocks were sampled along a transect across the west-central Great Basin (GB) in Nevada to the Ancestral Cascade Arc (ACA) in the northern Sierra Nevada, California (~39°–40° latitude), which are interpreted to represent a critical segment of a magmatic sweep that occurred as a result of subduction from east-northeast convergence between the Farallon and North American plates and extension related to the change from a convergent to a transform margin along the western edge of North America.

Mafic volcanic rocks from the study area can be spatially divided into three broad regions: GB (5–35 Ma), eastern ACA, and western ACA (2.5–16 Ma). The volcanic products are dominantly calc-alkalic but transition to alkalic toward the east. Great Basin lavas erupted far inland from the continental margin and have higher K, P, Ti, and La/Sm as well as lower $(Sr/P)_{pmn}$, Th/Rb, and Ba/Nb compared to ACA lavas. Higher Pb isotopic values, combined with lower Ce/Ce* and high Th/Nb ratios in some ACA lavas, are interpreted to come from slab sediment. Mafic lavas from the GB and ACA have overlapping $^{87}Sr/^{86}Sr$ and $^{143}Nd/^{144}Nd$ values that are consistent with mantle wedge melts mixing with a subduction-modified lithospheric mantle source. Eastern and western ACA lavas largely overlap in age and elemental and isotopic composition, with the exception of a small subset of lavas from the westernmost ACA region; these lavas show lower $^{87}Sr/^{86}Sr$ at a given $^{143}Nd/^{144}Nd$. Results show that although extension contributes to melting in some regions (e.g., selected lavas in the GB and Pyramid Lake), chemical signatures for most mafic melts are dominated by subduction-related mantle wedge and a lithospheric mantle component.

INTRODUCTION

The contrast between magmas derived at destructive plate margins and those at within-plate settings has long been explored (e.g., Hofmann et al., 1984; Ellam and Hawkesworth, 1988; Ormerod et al., 1991; Pearce and Peate, 1995; Pearce and Stern, 2006). The extensive tectonomagmatic geologic record of the North American Pacific margin includes orogenic events, passive and Andean-style convergent margins, hotspot magmatism, and extension (Dickinson, 2006, and references therein). Between ca. 45 Ma and ca. 3 Ma, a complex tectonic transition from subduction- to extension-related magmatism occurred in southwestern United States (e.g., Dickinson, 2006). Regionally, igneous activity in both the Great Basin (GB) and Ancestral Cascades Arc (ACA) consists of extensive magmatic events that migrated southwestward from western Utah to eastern California, commonly referred to as a "magmatic sweep" (Coney, 1978; Christiansen et al., 1992; Humphreys, 1995; Dickinson, 2006). The sweep of Cenozoic magmatism across the southwestern United States is thought to be due to the "rollback" of the shallow-dipping Farallon slap (i.e., sinking of the negatively buoyant slab into the asthenosphere and migration of the hinge line). Slab rollback caused the continental arc to retreat oceanward, inducing the southwestward magmatic sweep as the slab angle continued to steepen and volcanism migrated across the GB and transitioned into the ACA (Cousens et al., 2008; John et al., 2012). Volcanic eruptions began far from the continental margin (as far east as the San Juan volcanic field in Colorado, USA), include both mafic to intermediate lava flow complexes and rhyolitic caldera centers, and to date the mafic-intermediate lava complexes have received little attention in studies relevant to the origin and evolution of this migrating sweep of volcanism compared to caldera studies (e.g., Best et al., 2013; Henry and John, 2013). A segment spanning central western Nevada and eastern California was selected as the study area in order to examine the geochemical nature of mafic lavas extruded along the path of this magmatic sweep to address three issues: (1) origin of magmatism in the GB compared to the ACA, (2) changes in geochemistry over space and time, and (3) subduction- versus extension-related magmatism.

Geochemical studies of neighboring volcanic regions outside the study area are well represented in the literature, including the modern Cascade arc (e.g., Baker et al., 1994; Bacon et al., 1997; Green and

*Present address: Department of Earth Sciences, University of New Brunswick, 2 Bailey Drive, Fredericton, New Brunswick, Canada, E3B 5A3

Harry, 1999; Harry and Green, 1999; Borg et al., 2002; Strong and Wolff, 2003; Leeman et al., 2004; Green and Sinha, 2005), Yellowstone and the Snake River Plain (e.g., Camp, 1995; Christiansen et al., 2002; Jordan et al., 2004), the western Great Basin (WGB; Ormerod, 1988), the Mojave Desert and Basin and Range (e.g., Glazner et al., 1991; Perry et al., 1993; Farmer et al., 1995; Yogodzinski et al., 1996), and the San Andreas fault and offshore California (e.g., Cole and Basu, 1995; Davis et al., 1995; Dickinson, 1997). The ACA, located to the south of the modern Cascades, is also known as the Miocene–Pliocene Cascade Arc (Priest, 1990; Christiansen et al., 1992; Lipman, 1992; Dickinson, 1997, 2002, 2004; John 2001; Cousens et al., 2008; du Bray et al., 2009), with particular emphasis on the ACA within the Sierra Nevada (e.g., Putirka et al., 2012, and references therein). Late Cenozoic uplift of the southern Sierra Nevada is linked to ongoing delamination of the underlying lithospheric mantle based on geophysical (Wernicke et al., 1996; Wernicke and Snow, 1998; Boyd et al., 2004; Zandt et al., 2004), geological, and petrological work (Ducea and Saleeby, 1996, 1998; Manley et al., 2000; Ducea, 2001; Lee et al., 2001; Farmer et al., 2002; Lee, 2005; Putirka and Busby, 2007, 2011; Putirka et al., 2012). It should be noted that "lithosphere" is defined by McKenzie (1989) as "the mechanical boundary layer beneath the continental crust which remains physically isolated for geologically long periods from the convecting mantle beneath because it is relatively cold (so that heat passes through it entirely by conduction) and buoyant (due to chemical differentiation by melt extraction)." Thus the "asthenosphere" is the hot convecting upper mantle and is for the most part chemically separate from the lithosphere.

A lingering issue that plagues this region is whether or not the Eocene to late Pliocene "sweep" of magmatism across the GB was solely the result of subduction and rollback of the Farallon plate underneath the North American plate, or does extensional tectonism within the Basin and Range province after ca. 17 Ma also contribute to melt generation (e.g., Fitton et al., 1988; Ormerod et al., 1991; Asmerom et al., 1994; Yogodzinski et al., 1996)? Previous research from tectonomagmatic provinces within southwestern United States has determined specific geochemical signatures that represent subduction- versus extension-related processes. For example, lavas from the modern southern Cascades arc are calc-alkaline, dominantly intermediate in composition with enrichment in large-ion lithophile elements (LILEs) and light rare-earth elements (LREEs) and depletion in high field strength elements (HFSEs) (e.g., Borg et al., 1997). In contrast, eruptions due to extension in eastern California are commonly bimodal (basalt and rhyolite), high-K (typically) alkaline lavas, with higher $^{87}Sr/^{86}Sr$ and lower $^{143}Nd/^{144}Nd$ due to melting of the modified lithospheric mantle (e.g., Big Pine volcanic field, Ormerod et al., 1991), though proposed extension-related intermediate, trachyandesitic eruptions from volcanic centers such as the ca. 6 Ma Ebbetts Pass region (e.g., Hagan et al., 2009; Busby and Putirka, 2009) and Lake Mead (e.g., Weber and Smith, 1987) have been reported. In some cases, extension has thinned the lithosphere sufficiently that asthenosphere-derived magmatism allows alkali basalts with within-plate trace-element signatures to be emplaced (Reno-Fallon region, Buffalo Valley volcanic field, Lunar Craters volcanic field, and the Mojave Desert; Farmer et al., 1995; Cousens et al., 2012; Cousens et al., 2013; Rasoazanamparany et al., 2015).

Since primitive lavas (Mg# > 0.7, where Mg# = $Mg/(Mg + Fe^{2+})$) are rare in the GB-ACA region, the data have been filtered to include lavas with SiO_2 < 57 wt% and Mg# > 0.55, which limits the eastern reach of the east-west transect to the Stillwater Mountain Range within the central GB. This study offers a comprehensive geochemical investigation of the most "primitive" lavas erupted in an east-west transect across the GB to help understand the forces behind magma generation and tectonic evolution during 35 Ma to 3 Ma magmatic sweep (Fig. 1). A total of 98 basalts, basaltic andesites, and basaltic trachyandesites from the GB and the ACA were analyzed for petrography, detailed major- and trace-element contents as well as Sr, Nd, and Pb isotopic ratios to evaluate (1) mantle sources, (2) potential lithospheric and/or continental crustal contamination, and (3) variation in magmatic processes during the transition between subduction- and extension-related tectonic settings.

GEOLOGICAL SETTING

Regional Geological Setting

The tectonic history of southwestern North America has been described by several authors, including Lipman (1992), Atwater and Stock (1998), Sonder and Jones (1999), Henry and Ressel (2000), Dickinson (2002, 2006), and DeCelles (2004). Pre-Cenozoic rocks range in age from Precambrian to Mesozoic and almost all are meta-volcanic and meta-sedimentary (Bonham and Papke, 1969); all were subjected to the Antler (Late Devonian into the Mississippian), Sonoma (during the Permian/Triassic transition), Sevier (Jurassic to Eocene), and Laramide (Late Cretaceous to Eocene) orogenies (Dickinson, 2006; Mann, 2007). Subduction of the Farallon plate under the North American plate began during the Jurassic (Dickinson, 2006; Mann, 2007), and the North American coast underwent Andean-style arc volcanism centered in the Sierra Nevada arc until ca. 74 Ma. Subsequently, the arc front migrated several hundred kilometers inboard of the trench (Lipman, 1992), which is commonly referred to as the Laramide migration (ca. 70 to ca. 40 Ma) (e.g., Dickinson, 2006) because it accompanied the Laramide orogeny. The Laramide orogeny (ca. 80–35 Ma) is characterized by uplift of Precambrian crystalline basement due to the rapid, northeast-directed convergence between the Farallon and North American plates, whereas the Late Cretaceous Sevier orogeny is primarily characterized by thrusting and folding. During Laramide time, the relatively high convergence rate meant that the North American plate overrode the buoyant Farallon plate faster than the Farallon plate was able to sink. As a result, the Farallon plate was subducted beneath the North American plate at a very shallow angle, increasing the distance between the trench and the volcanic front (Lipman, 1992). In the literature, it is also proposed that uplift during the Laramide orogeny is the result of the shallow slab segment carrying a fragment of an aseismic ridge that was the counterpart of a large igneous province of the northwest Pacific basin named the Hess-Shatsky conjugate (Saleeby, 2003; Liu et al., 2010). Its thickened mafic crustal section relative to

abyssal lithosphere is presumed to have rendered a greater buoyancy leading to slab segmentation into the respective shallow domain (Saleeby, 2003).

By the late Cretaceous, the thickened and uplifted interior of western North America was tilted toward what is now referred to as the Sierra Nevada (Mitrovica et al., 1989; Humphreys et al., 2003), while the slab of younger and more buoyant lithosphere of the Farallon plate continued to subduct (Humphreys et al., 2003). This descending "flat slab" would have had a subduction angle of ~5° (Dumitru, 1991), creating traction on the base of the lithosphere, pulling it down, which caused the opening of the Cretaceous Seaway (Mitrovica et al., 1989), also called the Western Interior Seaway or North American Inland Sea. By mid-Eocene, the Farallon slab detached (Schellart et al., 2010) from the overriding lithosphere and "rolled back" (Best and Christiansen, 1991; Henry and Ressel, 2000; Dickinson, 2004, 2006; Best et al., 2016) along an east-northeast–trending axis, resulting in a southwestward magmatic "sweep" through Nevada before finally steepening to a "normal" (~30°) subduction angle (Coney and Reynolds, 1977; Dickinson and Snyder, 1978; Best and Christiansen, 1991; Dumitru, 1991; Seedorff, 1991; Hofstra et al., 1999; Henry and Ressel, 2000; Cline et al., 2005; Ressel and Henry, 2006). The magmatic sweep involved the emplacement of andesitic and dacite to rhyolitic ash flows and dome complexes (John, 2001), as well as small volumes of basaltic, andesitic, and dacitic lava as far east as the San Juan volcanic field in southwestern Colorado (Lipman et al., 1978). A northwest-trending belt of ash-flow calderas that developed through central Nevada is referred to as the "ignimbrite flare-up" (Best and Christiansen, 1991; John et al., 2008; Best et al., 2009; Best et al., 2016). Magmatic activity reached westernmost Nevada and eastern California between 20 and 17 Ma, forming major volcanic centers (e.g., Busby et al., 2008; Cousens et al., 2008; John et al., 2012). Between 17 and 14 Ma, subduction-related igneous activity in the Sierra Nevada and western Nevada was overlapped by rift or hotspot volcanism of the Northern Nevada Rift, Oregon High Plains, and Columbia River Flood Basalt provinces (Dickinson, 2006).

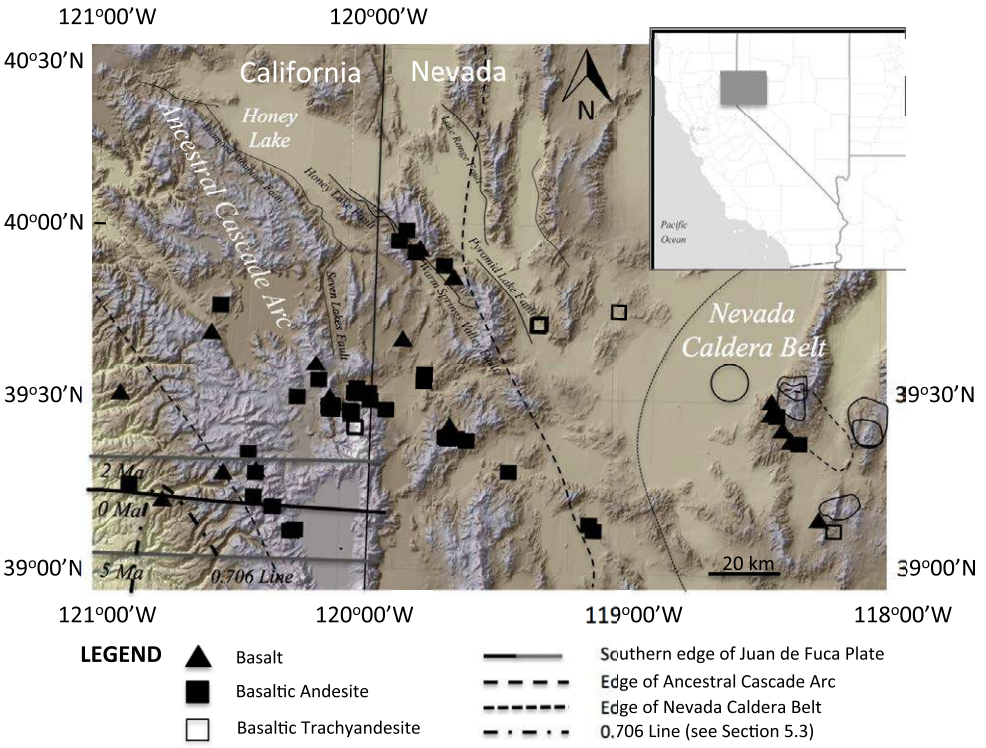

Figure 1. Simple digital elevation map of the study area and sample locations. The western edge of the Precambrian continental basement lies just outside of the study area, as is indicated by the 0.706 isopleth (modified from Kistler and Peterman, 1978). South edge of Juan de Fuca plate is also presented. The overlapping age from 4 Ma to present at latitude ~39.5° is because the slab edge is stationary beneath the Sierran–Great Valley block (see figure 11 from Atwater and Stock, 1998).

The latest geological chapter of the GB and ACA is occasionally referred to as an extensional orogeny (e.g., Elston, 1984). At ca. 28 Ma, the East Pacific Rise impacted the North American plate, bringing the Pacific plate into contact with the North American plate. A plate margin triple junction marked the initial point of contact of the Pacific, North American, and Farallon plates. The Farallon plate later split into smaller plates, which include the Juan de Fuca to the north (Mendocino Triple Junction [MTJ]) and Cocos plate to the south (Rivera Triple Junction [RTJ]). The MTJ has migrated northward such that the southern end of the volcanic (Cascade) arc associated with Cenozoic subduction beneath the North American plate has migrated northward since the Miocene (Atwater and Stock, 1998). Behind the arc, lithospheric extension began at ca. 17 Ma (Colgan et al., 2006a, 2006b) to form the GB, and migration of the GB into the Sierra Nevada mountains is an ongoing process (e.g., Manley et al., 2000; Kent et al., 2005).

Local Geological Setting

Samples of mafic rocks were collected over several field excursions from 1997 to 2011 between latitudes 39° and 40°. The area can be divided

longitudinally into three broad regions (Fig. 1): (1) the *GB* at approximate longitudes 117.00° to 119.52° (includes Stillwater Mountain Range, Truckee Range, Hot Springs Mountain, and Churchill Group), (2) the *eastern ACA* at approximate longitudes 119.52° to 120.00° (includes Sparks, Silver City, Pyramid, I-80 Suite, and Lousetown), and (3) the *western ACA* at approximate longitudes 120.00° to 121.00° (includes Stampede Reservoir, Ladybug, Portola, Mount Lincoln, Dog Valley, Stanford/Twin Peaks, Pond Terrace, Andesite Ridge, Devil's Peak, Boreal Ridge, Needle Peak, Squaw, Lowell Ridge, Sawtooth, Henness Pass, and Susanville) (Timmermans, 2015). Also included are geochemical and isotopic data for all three regions from Henry and Sloan (2003), Sloan et al. (2003), and du Bray et al. (2009). Petrographic descriptions for samples with the identifiers *04-LT* and *11-CN* are summarized in Table 1.

The Great Basin (GB)

The ***Stillwater Range*** is a ridge ~110 km long that trends north-northeast along the east side of Carson Sink, northeast of Fallon, Nevada. The southern Stillwater Range is composed of Tertiary igneous and non-marine sedimentary rocks (Fig. 2), that unconformably overlie, are faulted against, or intrude into faulted pre-Tertiary metasedimentary

TABLE 1. PETROGRAPHY OF MAFIC LAVAS FROM THE STUDY AREA WITH IDENTIFIERS 04-LT AND 11-LT

Sample	Rock type	% Phenocrysts				Matrix	Texture	Alteration
	Lavas	ol	px	pl	Fe-oxide			
Great Basin								
04-LT-51	Basalt	<5			<5	pl, px,ol, gl	Trachytic, vesicular, skeletal pl, vesicular, skeletal ol	c.i. of ol
04-LT-48	Basaltic trachyandesite		5	10–15	<5	holohyaline	Sieved pl	None
11-CN-26b	Basaltic trachyandesite			10	<5	pl, ol, gl	Textures and zonation inihibited by the extreme seritization	s. of pl (extreme)
11-CN-09	Basalt	5	5–10	20–25	<5	pl, ol, px, gl	Subophitic, minor (<5%) zoned pl, minor (<5%) sieved pl	None
04-LT-41	Basaltic andesite	<5	5	10–15	<5	pl, px, ol, gl	Seriate or three stages of pl growth, largest pl sieved and zoned	c.i. of ol
04-LT-42	Basalt	<5		10	Trace	pl, px ,ol, gl	Zoned pl, sieved pl, groundmass is trachytic, subophitic	p.i. of ol
04-LT-06	Basaltic trachyandesite	<5	<5		<5	pl, ol, px, mt, gl	Phenocrysts very small (microcrysts), vesicular, trachytic	p.i. of ol
04-LT-02	Basaltic trachyandesite	<5			<5	pl, ol, px, mt, gl	Trachytic	p.i. of ol
04-LT-05	Basaltic trachyandesite	<5	5–10		5	pl, ol, px, mt, gl	Zoned pl	p.i. of ol
04-LT-08	Basaltic trachyandesite	<5		5		pl, ol, px, mt, gl	Glomeroporphyritic	p.i. of ol
04-LT-09	Basaltic trachyandesite	5–10		10–15	Trace	gl, pl, ol, px	Trachytic	c.i. of ol
04-LT-10	Basaltic trachyandesite	<5		<5	<5	pl, ol, px, gl	Trachytic	c.i. of ol
Eastern Ancestral Cascade Arc								
04-LT-32	Basaltic andesite	5–10			5	pl, ol, mt, gl	Embayed ol, trachytic	Rimmed ol
04-LT-31	Basaltic andesite	<5			5	pl, px, ol, mt	Embayed ol, trachytic	p.i. of ol
04-LT-25	Basaltic andesite			5	5	pl, ol, px, mt	Seriate pl,	p.i. of ol, Sericite
04-LT-24	Basaltic andesite	5–10	5	15–20	5	pl, ol, px, mt	Zoned pl, sieved pl	p.i. of ol
Western Ancestral Cascade Arc								
04-LT-01	Basaltic andesite	15	10	<5		pl, px, mt, gl		
04-LT-87	Basaltic andesite	10			<5	pl, ol, mt, gl	Embayed ol	
04-LT-83	Basalt	10	10	<5		pl, ol, px, mt, gl		p.i. of ol
04-LT-21	Basaltic andesite	<5	5–10	<5	Trace	pl, px, gl	Zoned pl, sieved pl, embayed sometimes rimmed ol, trachytic	
04-LT-17	Basaltic trachyandesite				5	pl, mt, ol, gl	Aphyric, hypocrystalline	c.i. of ol
04-LT-68a	Basalt							
04-LT-98	Basaltic andesite							

Minerals: ol—olivine; px—pyroxene; pl—plagioclase; mt—magnetite; gl—glass. Alteration: p.i.—partial iddingsitization; c.i.—complete iddingsitization; s.—saussuritization.

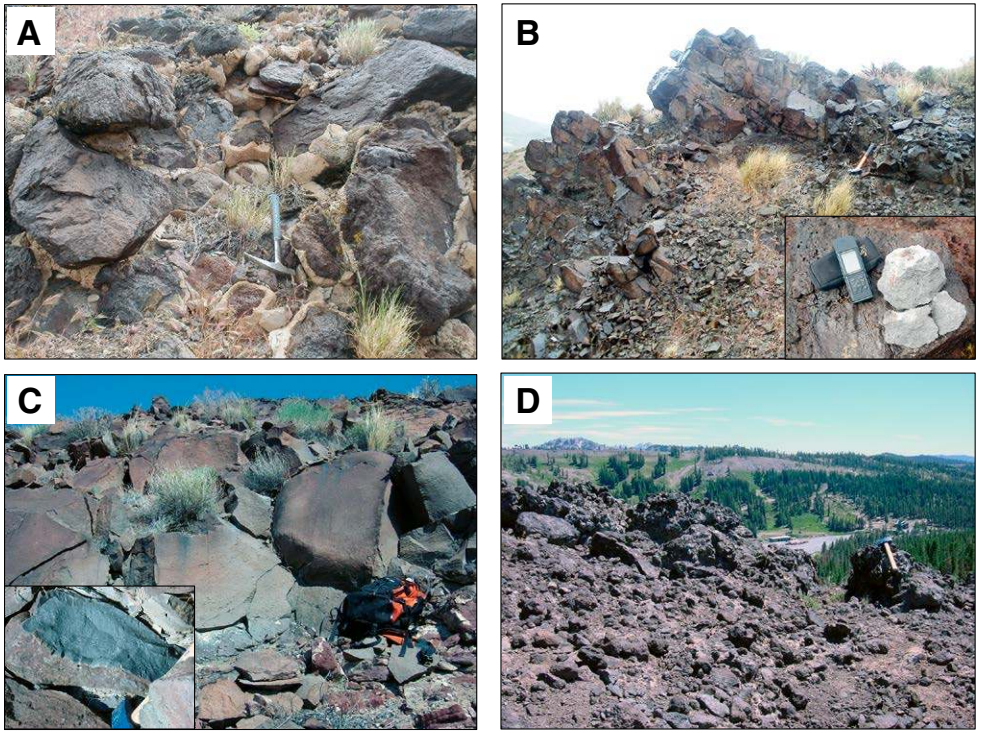

Figure 2. Photos from the field area: (A) basaltic boulders encapsulated in tufa from the southwest side of the Stillwater Mountain Range (Great Basin [GB]); (B) basalt from same location as (A) at higher elevation (free of tufa); (C) basaltic trachyandesite from the Truckee Range (GB); and (D) basaltic andesite from Andesite Ridge (western Ancestral Cascade Arc [ACA]). Rock hammer is ~35 cm in length, and the GPS is ~15 cm in length.

and metavolcanic basement rocks (Page, 1965; John, 1995). The region was later subjected to Miocene structural tilting and extensional faulting (Page, 1965; John, 1995). Miocene basalt and basaltic andesite occur at various sites including the volcanic fields near Mountain Well Road and La Plata Canyon. Jurassic lavas from the Stillwater Range show higher levels of hydrothermal alteration causing extreme saussuritization of plagioclase to primarily sericite, calcite, and chlorite compared to Tertiary lavas. Seriate texture is present in sample 04-LT-41, whereas other lava flows show at least two stages of feldspar growth. Basalt from La Plata Canyon is aphyric and plagioclase rich. ***Bell Canyon*** is situated southeast of the Stillwater Range and encompasses most of a range that includes Fairview Peak and the northern part of Slate Mountain (Henry, 1996). Rock units include Jurassic to Triassic metamorphic rocks intruded by Cretaceous granodiorite, a wide range of Oligocene to Miocene volcanic and volcaniclastic rocks (most of which are related to a ca. 19 Ma caldera), and upper Neogene to Quaternary sedimentary deposits. Vitrophyric basaltic andesitic lava flows and dikes have 25% phenocrysts of plagioclase and olivine in a hyalocrystalline groundmass (Fig. 3A). The basaltic unit (04-LT-51) has basal scoria breccia that develops into a massive but highly vesicular lava with 20% phenocrysts of plagioclase, clinopyroxene, and iddingsitized olivine (Henry, 1996). A sample from Bell Canyon (04-LT-48) has a holohyaline groundmass.

The ***Hot Springs Mountain*** and the ***Truckee Ranges*** lie in west-central GB abutting against the Walker Lane (Bonham and Papke, 1969). They comprise a series of hills that form part of the northwestern boundary of the large Carson Sink depression. Exposed rocks in the region range from Triassic to Holocene (Willden and Speed, 1974). Cenozoic rocks are primarily volcanic and consist of alternating sequences of flows, tuffs, and shallow intrusive rocks. Lavas are basaltic trachyandesites that commonly contain abundant plagioclase and minor olivine and/or augite phenocrysts (Fig. 3C). Olivine is generally euhedral and mildly to completely altered to iddingsite. Subhedral augite commonly shows subophitic texture with plagioclase, and most include plagioclase phenocrysts with sieve texture and oscillatory or normal zonation (Fig. 3B).

Eastern and Western Ancestral Cascades Arc (Eastern and Western ACA)

The pre-Cenozoic rocks are mainly Mesozoic granitoids with minor Paleozoic metasedimentary and metavolcanic rocks (Ashley et al., 1979). A series of intermediate magmatic events that occurred between 17 and 12 Ma resulted in several formations including Kate Peak, Alta, and Truckee formations (Ashley et al., 1979). Magmatism that began again at ca. 10 Ma (Cousens et al., 2008) consisted of more mafic compositions ranging from pyroxene andesite to olivine-pyroxene basalt. Basalts from the eastern and western ACA are primarily porphyritic with olivine and/or augite phenocrysts. Basaltic andesites are mineralogically similar to the basalts, although plagioclase dominates over olivine and sparse microphenocrysts of orthopyroxene and/or clinopyroxene (Cousens et al., 2008). Plagioclase phenocrysts (as much as 15% by volume) typically occur as glomerocrysts that are either zoned with resorbed interiors or, more commonly, are zoned and subhedral. Smaller feldspar grains are skeletal to euhedral and generally lack zoning.

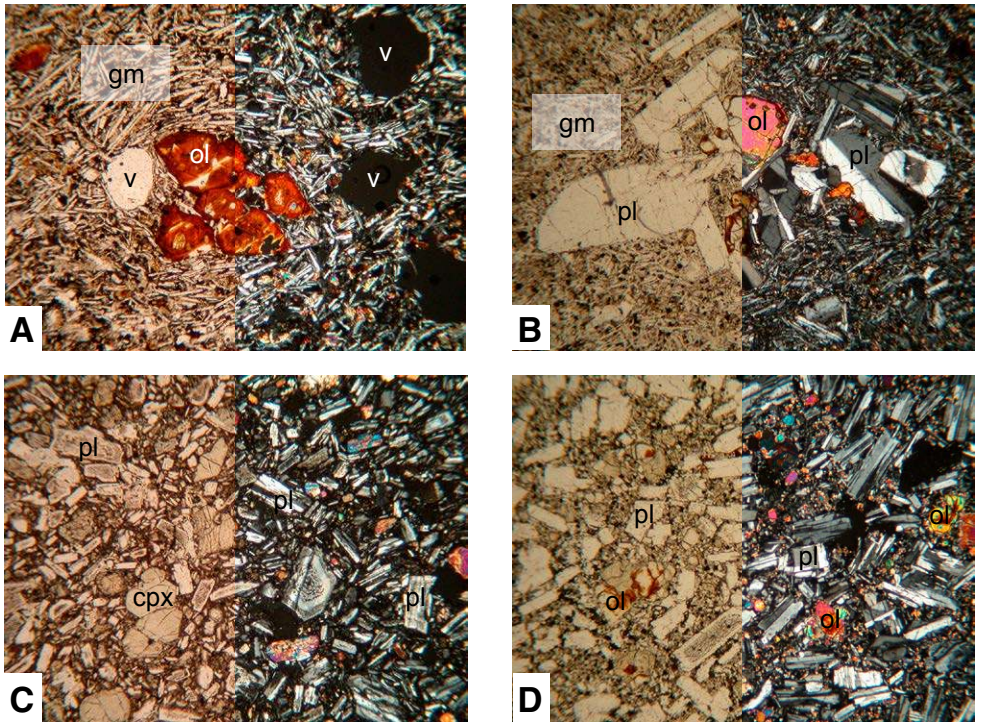

Figure 3. Thin section photos of various mafic lavas from the study area. Each thin section has been divided: the left side shows the rock in plane polarized light (PPL), and the right side shows crossed polarized light (XPL). (A) Sample 04-LT-51 is a basalt from Bell Canyon in the Great Basin (GB). (B) Sample 04-LT-08 is a basaltic trachyandesite from the Truckee Range in the GB. (C) Sample 04-LT-21 is a basaltic andesite from the Andesite Ridge in the western Ancestral Cascade Arc (ACA). (D) Sample 04-LT-24 is a basaltic andesite from Lousetown in the eastern ACA. Abbreviations on photos: v—vesicle, ol—olivine, pl—plagioclase, cpx—clinopyroxene, gm—groundmass.

Sparks is located to the north of the town of Sparks, just east of Reno. Mafic lavas from Sparks are basaltic andesites that contain phenocrysts of clinopyroxene, plagioclase, and iddingsitized olivine. The extensive ***Lousetown*** Formation, southwest of Reno, covers ~40 km² in the Virginia City quadrangle, and extends into the Mount Rose, Wadsworth, and Churchill Butte quadrangles (Ashley et al., 1979). The ***I-80 Suite*** refers to lavas with similar ages (<10 Ma) and chemical and physical characteristics that are located along the Interstate-80 corridor between north Lake Tahoe and Reno (Henry and Perkins, 2001; Cousens et al., 2008). ***Ladybug Peak,*** at the north end of Verdi Range, represents an explosive and effusive episode of mafic volcanism (Cousens et al., 2008) that may be related to the region's 12–10 Ma extensional event (Henry and Perkins, 2001; Henry et al., 2011). These basalts and basaltic andesites contain as much as 15% olivine grains up to 4 mm in size, 10% augite up to 2 mm in size, and minor plagioclase set in a fine-grained matrix of feldspar and pyroxene (Cousens et al., 2008).

The ***Pyramid Sequence*** (ca. 13 Ma), located to the southeast of Pyramid Lake, consists primarily of interbedded basalt to basaltic andesite, sparse andesitic lavas and rare rhyolitic lava, coarse- to fine-grained clastic rocks, and a dacitic ash-flow tuff (Henry et al., 2004a). The mafic lavas considered range from aphyric to coarsely porphyritic. The coarsely porphyritic rocks are characterized by prominent, tabular plagioclase phenocrysts up to 20 mm long and 2–4 mm wide (Henry et al., 2004a).

Younger (ca. 3 Ma) and mildly phyric, olivine-clinopyroxene basaltic andesites, and basaltic trachyandesites were extruded atop the northern ***Carson Range,*** just south of Reno. The northern end of the Carson Range is composed primarily of tilted, porphyritic lavas capped by gently dipping to flat-lying, poorly phyric lava flows (Thompson and White, 1964; Latham, 1985). Samples 01-LT-10, -11 (basaltic andesites), and -12 (basaltic trachyandesite) are from a set of flows near Fuller Lake. Samples 01-LT-10 and -11 contain altered olivine and rare plagioclase phenocrysts, whereas sample 12 is much fresher with minor olivine and pyroxene phenocrysts. Locations for samples 01-LT-46–53 are included in Cousens et al. (2011). These samples commonly include minor olivine phenocrysts, with or without minor plagioclase and pyroxene phenocrysts, in a trachytic matrix. The basaltic and basaltic andesitic lava flows of ***Dog Valley*** (4–3 Ma) are located just west of the Carson Range.

Samples from ***Pond Terrace, Andesite Peak, Devil's Peak***, ***Mount Lincoln, Twin Peaks***, ***Stanford Peak***, ***Squaw Peak, Sawtooth***, and ***Henness Pass*** are from highly eroded volcanic complexes emplaced 8–6 Ma and 5–3 Ma that cap high Sierra Nevada granitoid intrusions from the west side of Lake Tahoe north to Donner Pass (Harwood, 1981; Saucedo and Wagner, 1992; Henry et al., 2004b; Cousens et al., 2008). The volcanic rocks of this area include lava flows, agglomerates, tuffs, and plug intrusions of lava and breccia (Hudson, 1951), as well as volumetrically minor amounts of olivine-clinopyroxene basalt and basaltic andesite lava flows (Henry et al., 2004b; Cousens et al., 2008). At Squaw Peak and Mount Lincoln, debris lava flows and dome-collapse deposits are composed of fragments of plagioclase-phyric volcanic rock set in a mineralogically similar volcanic matrix. Subordinate lava flows are commonly >10 m thick, massive, and highly plagioclase porphyritic. Some basaltic andesites, particularly those in the Squaw–Twin Peaks area, include abundant

anhedral sieve-textured plagioclase grains that may be xenocrystic. Trachytic texture in the groundmass is less common in the basaltic andesites compared to the basalts. Farther north into the Sierra Nevada along Highway 70, basalts and basaltic andesites from ***Portola*** contain phenocrysts of embayed olivine and rare augite in a hypocrystalline matrix of plagioclase and olivine.

In general, the mafic lavas with Mg# > 0.55 closely follow the idealized olivine-clinopyroxene fractionation trend (Harker, 1909). Many of the lavas contain phenocrystic olivine and clinopyroxene along with plagioclase, implying that the initial magma evolution was at relatively high pressure under hydrous and/or non-hydrous conditions (>8 kbar, Green and Hibberson, 1970; Green et al., 2010).

The western ACA is located almost entirely in the unextended Sierra Nevada, whereas the eastern ACA includes volcanic rocks that were emplaced in terranes adjacent to the Sierra Nevada that either were subsequently faulted and rotated or were emplaced into terrane that was undergoing extensional faulting and deformation. Did extension in the eastern ACA allow for different mantle sources to be tapped than did the unextended Sierra Nevada? Or do the similar basement rocks in both western and eastern ACA control mantle sources and petrogenetic evolution in lavas emplaced in either part of the arc?

METHODOLOGY

Field Work and Data Sources

Locations of mafic volcanic rocks between 40 and 3 Ma in age were determined using existing geologic maps: Page (1965), Stewart and Carlson (1976), Bell and Bonham (1987), Henry (1996), Jones (1997), Stewart (1999), Henry et al. (2004c), Saucedo et al. (2005), Castor et al. (2006), Hudson et al. (2009), and Bell et al. (2010). Ice sheets from Pleistocene glacial events reached well into the southwestern United States, leaving only remnants of lava flows, debris flows, and volcanic necks. Bedrock is for the most part well exposed, though outcrops within the GB suffer from higher degrees of weathering compared to the ACA (Fig. 2). Figure 1 shows the sample locations; a complete list of sample names and locations (note: samples were located using a handheld global positioning system [GPS] and GPS coordinates) is presented in Timmermans (2015) and Supplemental Table S1[1].

Samples with identifiers 04-LT and 11-CN were collected by the authors during two field seasons in 2004 and 2011, respectively, for the purpose of filling data gaps along the east-west transect. Sampling was occasionally obstructed by middle to late Pleistocene lacustrine and interlacustrine deposits—the result of several glacial episodes that also eroded the Sierra Nevada Mountain landscape (Morrison, 1964). Outcrops surrounding the Carson Sink (e.g., Lahontan Mountains, Stillwater Mountain Range) are commonly shoreline deposits encrusted by tufa (carbonate deposits formed by precipitation from saline lake water due to significant departure from ambient temperature), deposited along the margin of a large endorheic lake named Lake Lahontan (Morrison, 1964). Samples from these regions were collected from outcrops above the ancient shorelines.

Existing published data from the region were included in the database for this study. Samples with identifiers LT and Towle were collected between 1997 and 2008 by Brian Cousens, Julie Prytulak, and Russell Towle. Hand samples, thin sections, and geochemistry data from these specimens were all processed and analyzed at Carleton University, Ottawa, Ontario. Sample data with all other identifiers were obtained from Henry and Sloan (2003), Sloan et al. (2003), du Bray et al. (2009), and geochemical databases, for which only the geochemical data were adopted.

Geochronology

Ages for the mafic samples used are based on radiometric ages determined for samples or sample localities. Radiometric ages were primarily derived from $^{40}Ar/^{39}Ar$ geochronology from the Nevada Bureau of Mines and Geology (NBMG) using methodology as described in detail by Henry et al. (1996) and Henry et al. (1997). Ages are rounded to the nearest million years (du Bray et al., 2009).

Geochemistry

Geochemical data are listed in Supplemental Table S1 (footnote 1). Collected samples from the GB and ACA were prepared at Carleton University, Ottawa. Rock samples were slabbed, crushed in a Bico chipmunk jaw crusher, and ground to a fine powder in either an agate or a chromium-steel ring mill. Between samples, the jaw crusher and the ring mill were cleaned thoroughly using water, compressed air, and ethyl alcohol. Replicate analyses for 11-CN-1 and 11-CN-11 through a chrome-steel and an agate ring mill have been compared, indicating only minor Cr contamination for splits processed through the chrome-steel head. Whole-rock major- and trace-element contents were determined by fused-disc X-ray fluorescence spectrometry (XRF; University of Ottawa) and solution mode inductively coupled plasma mass spectrometry (ICP-MS; Ontario Geological Survey, Sudbury). The precisions of the data, based on replicate analyses of samples and blind standards, are listed with the data presented in Supplemental Table S1 (footnote 1). Detection limits indicate the minimum concentration that can be distinguished from a blank specimen; values were calculated by personnel at the Ontario Geological Survey Geoscience Laboratories.

All Pb, Sr, and Nd isotopic ratio analyses and sample preparations, including weighing, acid washing, dissolution, column chromatography, filament loading, and mass spectrometry, were performed at the Isotope Geochemistry and Geochronology Research Centre (IGGRC) at Carleton University, Ottawa, Canada, using techniques presented in Cousens (1996). For samples processed before 2002, samples were run on a Finnigan-MAT 261 thermal ionization mass spectrometer run in static mode. Strontium was loaded onto a single Ta filament with H_3PO_4. Isotope ratios were normalized to $^{86}Sr/^{88}Sr = 0.11940$. Two standards were run: National Institute of Standards and Technology (NIST) standard reference material (SRM) 987 ($^{87}Sr/^{86}Sr = 0.710257 \pm 0.000022$) and the Eimer and Amend (EandA) $SrCO_3$ ($^{87}Sr/^{86}Sr = 0.708035 \pm 0.000010$). Neodymium was loaded with H_3PO_4 on one side of a Re double-filament assembly. Isotope

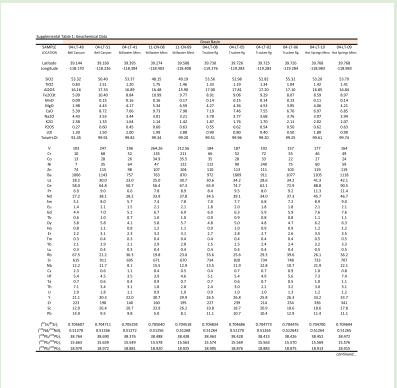

[1]Supplemental Tables. Sample locations, GPS coordinates, and geochemical data. Please visit https://doi.org/10.1130/GEOS.S.12233756 to access the supplemental material, and contact editing@geosociety.org with any questions.

ratios are normalized to $^{146}Nd/^{144}Nd = 0.72190$. Analyses of the La Jolla standard average $^{143}Nd/^{144}Nd = 0.511874 \pm 0.000019$. Lead was loaded onto single Re filaments with H_3PO_4 and silica gel. All mass spectrometer runs were corrected for fractionation by monitoring NIST SRM 981 (Todt et al., 1996). The average measured ratios for SRM 981 are $^{206}Pb/^{204}Pb = 16.890 \pm 0.012$, $^{207}Pb/^{204}Pb = 15.429 \pm 0.014$, and $^{208}Pb/^{204}Pb = 36.502 \pm 0.048$. Lead concentrations are precise to ±0.5%. Analysis of U.S. Geological Survey (USGS) standard BCR-1 yields Pb = 13.56 ppm, $^{206}Pb/^{204}Pb = 18.818$, $^{207}Pb/^{204}Pb = 15.633$, and $^{208}Pb/^{204}Pb = 38.633$.

For samples processed after 2002, samples were run on the Thermo Finnigan Triton TI thermal ionization mass spectrometer. Strontium isotope ratios were normalized to $^{87}Sr/^{88}Sr = 0.11940$, and the lab average for NBS 987 was $^{87}Sr/^{86}Sr = 0.710248 \pm 0.000026$. Neodymium isotope ratios are normalized to $^{146}Nd/^{144}Nd = 0.72190$, and runs of the La Jolla standard averaged $^{143}Nd/^{144}Nd = 0.511877 \pm 0.000018$. All Pb ratio mass spectrometer runs are corrected for fractionation relative to the following accepted values for NIST NBS 981: $^{206}Pb/^{204}Pb = 16.937 \pm 0.009$, $^{207}Pb/^{204}Pb = 15.492 \pm 0.008$, and $^{208}Pb/^{204}Pb = 36.722 \pm 0.019$ (Todt et al., 1996). All quoted uncertainties are 2 standard deviations of the mean.

RESULTS

Low loss-on-ignition (LOI) values (<3 wt%) and petrological observations indicate that secondary processes have not significantly affected the collected samples. Secondary minerals such as sericite and chlorite are rarely seen during petrological examination. LOI data are also good proxies to discriminate between fresh and weathered samples when compared to La/Sm values, for which correlation was observed for the ACA and the GB lavas (not shown) (Labanieh et al., 2012). This lack of correlation implies that weathering did not have a significant effect on the REEs in the studied samples (Yusoff et al., 2013).

Mafic lavas that erupted within the east-west transect exhibit a wide range of compositions and significant variations among and within the eruptive centers. Subalkaline lavas are found throughout the study area (Fig. 4; Le Bas et al., 1986). The Mg/(Mg + Fe^{2+}) ratios (where $Fe^{2+}/Fe_{tot} = 0.9$), represented as the Mg#, range from 0.75 to 0.55, indicating that although some of the mostly subalkaline mafic lavas are near-primary melts (that is, if mantle olivine is $Fo_{86–90}$, primary magmas must be Mg# = 0.68–0.75) (e.g., mafic samples from the western ACA, Mg# > 0.65; Le Bas et al., 1986), most lavas have undergone some postgeneration modification. Figures 5A–5F and 6 show variation diagrams, where major and trace elements are plotted against Mg#. In general, basalts, basaltic andesites, and basaltic trachyandesites from the GB have an overall lower Mg# (0.55–0.65) than those from the eastern and western ACA (up to 0.75 in the case of the western ACA). Basalts with Mg# > 0.7 also have Cr > 600 ppm, Ni > 180 ppm, and Sc > 32 ppm. The AFM (alkalis-FeO-MgO) diagram (not shown, Irvine and Baragar, 1971) shows that most mafic lavas plot primarily in the mafic field along a calc-alkaline trend. The GB lavas have higher $Fe_2O_3^t/MgO$ values compared to the ACA lavas. The concentrations of Ni, Cr, and Sc all decrease with decreasing Mg#, along with CaO/Al_2O_3, indicating that olivine, Cr-spinel, and clinopyroxene in the ACA lavas were dominant crystallizing mineral phases. Al_2O_3 contents range from 13 wt% to as high as 20 wt%, with the eastern ACA containing the highest Al_2O_3 and the least scatter. K_2O values range from 0.5 wt% to as high as 2.5 wt% (sample 01-LT-12 from the Carson Range trends to shoshonitic affinities). The TiO_2, P_2O_5, K_2O, REEs, Zr, and Y contents all increase with decreasing Mg# and are notably higher in lavas from the GB. The decrease in transition metal (V, Ni, Co, and Cu) abundances during fractional crystallization is principally a function of the precipitation of olivine, Fe-Ti oxides (crystallization of Fe-Ti oxides is largely governed by the melt redox state), and immiscible sulfides. Vanadium generally decreases only slightly with decreasing Mg#, confirming together with increasing TiO_2 that for mafic melts, Fe-Ti oxides are not a dominant fractionating phase, which agrees with experimental studies for primitive lavas at oxygen fugacities typical for arcs (e.g., Lee, 2005). Large-ion lithophile

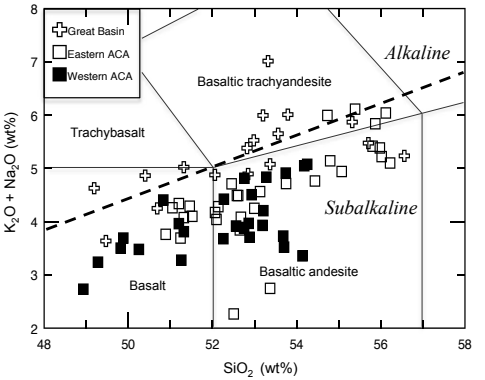

Figure 4. Alkali-silica diagram (modified from Le Bas et al., 1986) for mafic lavas from the Great Basin (GB) and eastern and western Ancestral Cascade Arc (ACA).

element abundances for different localities generally do not co-vary with Mg#. Isolated flows of basalt and basaltic trachyandesite from the GB (in the Bell Mountains and the Stillwater Range) are characterized by similar SiO_2 and K_2O but lower Mg#, higher P_2O_5, TiO_2, and Zr relative to the more abundant subalkaline basalts. These slightly alkaline lavas generally have higher REE abundances compared to the subalkaline basalts. The basaltic trachyandesites are very uniform in composition and are generally enriched in TiO_2, K_2O, P_2O_5, Rb, Ni, Zr, Nb, Pb, Zr/Y, and the REEs compared to the subalkaline basalt and basaltic andesite groups.

Figure 7 compares (A) Zr/Yb and (B) Th/Yb with Nb/Yb. Mafic melts generally possess only a small range of Yb contents, whereas the Nb contents can reflect variations from the source (Pearce, 2008). All samples plot above the mid-ocean ridge basalt–ocean island basalt (MORB–OIB) array, indicating that they derived from mantle contaminated by either a slab fluid or continental crust (higher Th/Yb) or a continental lithospheric mantle (CLM) component (higher Zr/Yb). The ACA lavas trend parallel to the MORB-OIB array in Figure 7B, indicating the importance of melt extraction during subduction in an arc system (Pearce and Peate, 1995). The GB lavas, however, do not parallel the array, which may indicate that the higher Th/Yb values (Fig. 7B) are derived from another source. Comparing Zr/Yb

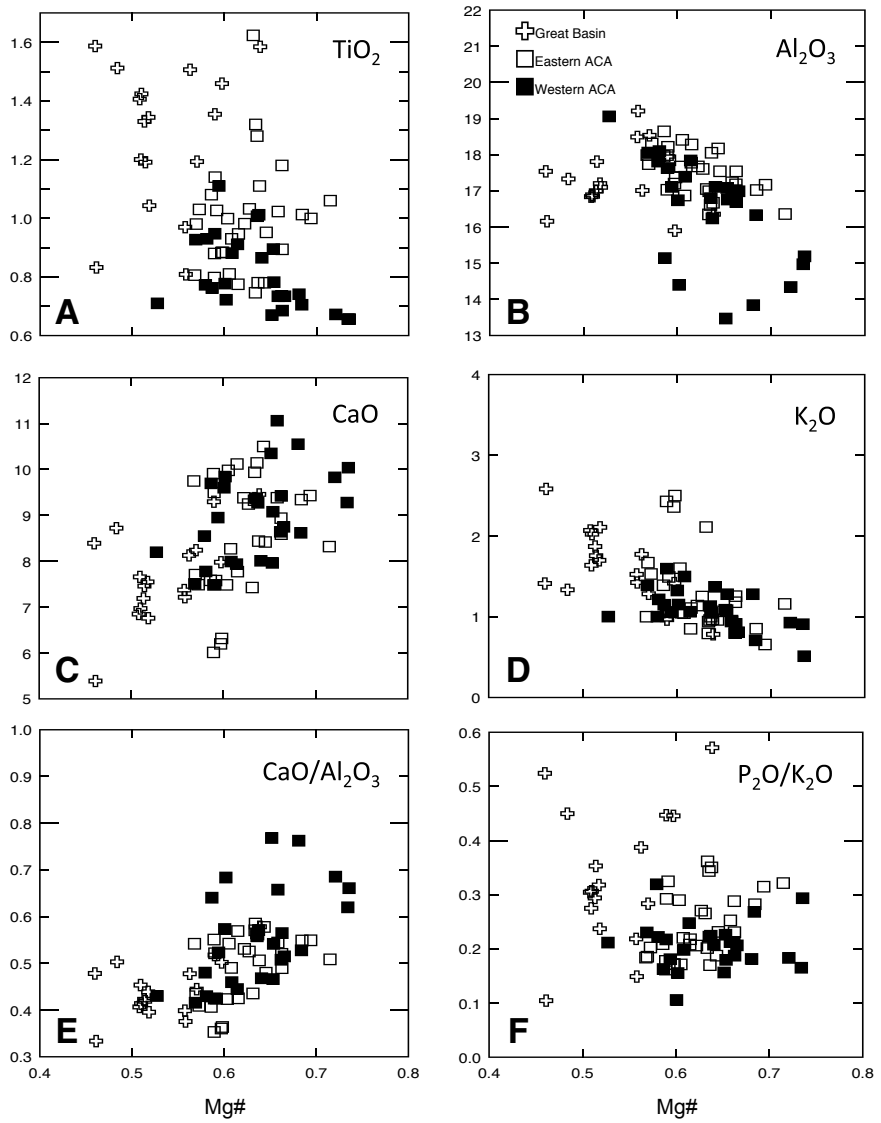

Figure 5. Plots A to F show major element versus Mg# for the Great Basin (GB), eastern Ancestral Cascade Arc (ACA), and western ACA regions from the study area (see legend). See text for discussion.

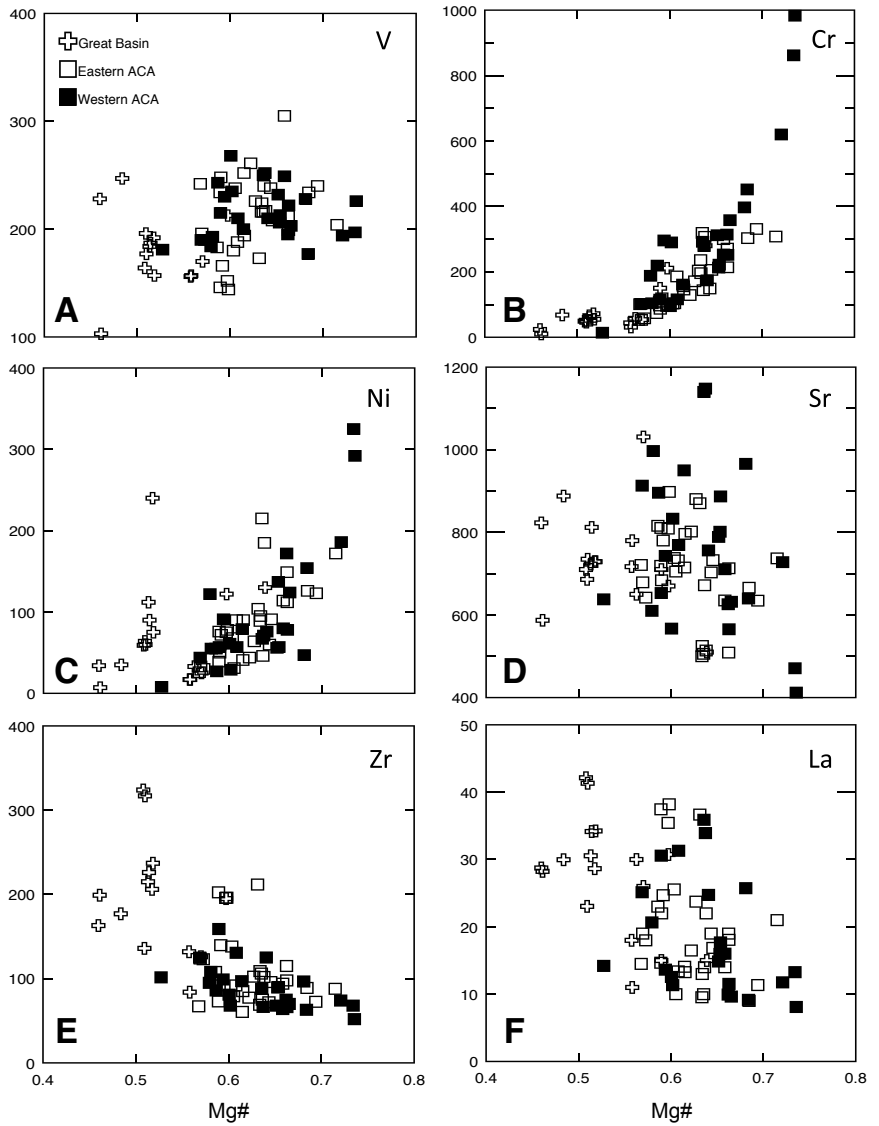

Figure 6. Trace-element Harker plots for the Great Basin (GB) (open cross), eastern Ancestral Cascade Arc (ACA) (open square), and western ACA (filled square) regions from the study area (see legend) (Harker, 1909). See text for discussion.

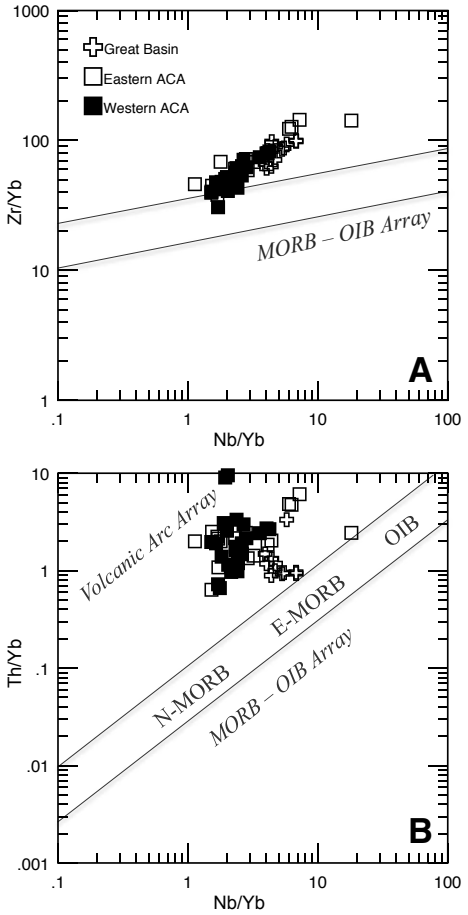

Figure 7. Mafic lavas from the Great Basin (GB) and Ancestral Cascade Arc (ACA) plotted along the various end members as defined in Pearce (2008). See text for further discussion. Abbreviations: E-MORB—enhanced mid-ocean ridge basalt; N-MORB—normal mid-ocean ridge basalt; OIB—ocean-island basalt.

with Nb/Yb (Fig. 7A), most lavas from the eastern ACA and the western ACA have Zr/Yb values that also lie within and slightly above the MORB array, whereas the GB lavas trend toward the E-MORB or OIB mantle array (Pearce and Peate, 1995; Pearce, 2008). Younger (ca. 3 Ma) basaltic trachyandesites from the Carson Range lie outside the eastern ACA and the western ACA fields (basalts and basaltic andesites) with comparatively higher La/Yb, Th/Yb, Zr/Yb, and Nb/Yb values than other lavas.

Rare-earth and trace-element concentrations (Figs. 8 and 9) have been normalized to chondritic and primitive mantle abundances of Sun and McDonough (1989), respectively. The three regions are represented separately by symbols representing composition. All lavas have primitive mantle normalized La/Sm between 2 and 3.7; however, the GB lavas have a more restricted range (2.4–3.6) than the ACA lavas. All GB lavas show higher abundance in all REEs with no fractionation of the light rare earth elements (LREE) and/or heavy rare earth elements (HREE). The GB lavas also have negative Eu-anomalies that increase with increasing REE abundance to a maximum of Eu/Eu* = 0.77. Eu anomalies are denoted by Eu/Eu* and calculated as $(Eu/Eu^*)_{pmn} = Eu_{pmn}/((Sm_{pmn} + Gd_{pmn})/2)$. The REE patterns in Figure 8A show that all GB lavas share parallel REE patterns but vary in overall abundance. For the eastern ACA lavas (Fig. 8B), normalized values are variable from La to Sm, but then the REE patterns converge toward the HREEs, forming a fanning set of patterns. The western ACA lavas (Fig. 8C) show a lower range of La to Sm ratios compared to the eastern ACA lavas; however, both groups of ACA lavas show variations in light REE abundance but have relatively flat middle to heavy REE patterns (mean values for GB, eastern ACA, and western ACA shown in Fig. 8D). Lavas with higher silica and alkali contents generally have higher REE abundances and higher La/Sm ratios compared to lavas with lower silica and alkali contents. All samples show a slight negative anomaly (Eu/Eu* = 0.997–0.768, average 0.911) with lavas from the GB containing the largest Eu anomalies (averaging 0.834). Basaltic trachyandesites from Hot Springs Mountain (GB) have the overall largest Eu anomaly of 0.768. A basalt from Portola and a basaltic andesite from Stanford/Twin Peaks, both from the western ACA, have an atypical negative Ce-anomaly (Ce/Ce* = 0.849 and 0.713, respectively), where Ce/Ce* anomalies are calculated $Ce/Ce^* = Ce_{pmn}/((La_{pmn} + Pr_{pmn})/2)$. All other samples have Ce-anomalies that hover just under 1 (average 0.954).

Most trace-element patterns show large enrichments in LILEs (e.g., Ba, Rb, K, and Pb) and lesser enrichments in LREEs (e.g., La, Ce, Nd, and Sm) relative to HFSEs (e.g., Nb, Ti, and Ta) and heavy rare-earth (HRE, e.g., Tb, Tm, and Yb) elements, characteristic of arc magmas (Figs. 9A–9C) (Gill, 1981; Pearce, 1983; Rollinson, 2014; Briqueu et al., 1984; Weaver et al., 1987). The subduction signature seen in Figure 9 (i.e., depletion in Nb and Ta and enrichment in LILEs when compared to the primitive mantle) is strongest in the western and selected eastern ACA and weakest in the GB (Fig. 9D). The eastern and western ACA mafic rocks show a larger Sr enrichment relative to Nd compared to the GB.

Isotopic compositions of Sr, Nd, and Pb have been measured for select samples from the GB and the eastern and western ACA, the results of which are shown in Figure 10 and listed in Supplemental Table S1 (footnote 1). Isotopically, the groups are highly heterogeneous with the western ACA containing the widest range: $^{87}Sr/^{86}Sr = 0.70381–0.70612$ and $^{143}Nd/^{144}Nd = 0.51242–0.51283$. The eastern ACA and the GB have more restricted ranges: $^{87}Sr/^{86}Sr = 0.70411–0.70552$ and $^{143}Nd/^{144}Nd = 0.51261–0.51272$, $^{87}Sr/^{86}Sr = 0.70453–0.70531$ and $^{143}Nd/^{144}Nd = 0.51262–0.51283$, respectively (Fig. 10A). The isotopic ratios overlap for the GB, part of I-80 Suite, Sparks, Carson Range, Lousetown, Henness Pass, and Susanville (eastern and western ACA). Note that six samples from the westernmost part of the ACA, along the crest of the Sierra Nevada, plot to the left of the main array of mafic lavas: i.e., at low $^{87}Sr/^{86}Sr$ given their $^{143}Nd/^{144}Nd$. These lavas include Mount Lincoln basalt, Squaw Peak, Pond Terrace, Devil's Peak, and Lowell Ridge; subsequently, these flows will be referred to as the *westernmost part of the ACA* (circled in Fig. 10A). However, other lavas from the Sierra Nevada crest plot within the main data array.

Lead-isotope compositions for mafic lavas are also heterogeneous, shown in Figures 10B and 10C relative to the Northern Hemisphere Reference Line (NHRL) for oceanic basalts from the Northern Hemisphere (Hart, 1984). The GB and the ACA lavas range in $^{206}Pb/^{204}Pb$ between 18.85 and 19.15, $^{207}Pb/^{204}Pb$ between 15.52 and 15.69, and $^{208}Pb/^{204}Pb$ between 38.33 and 38.97. For $^{207}Pb/^{204}Pb$ versus $^{206}Pb/^{204}Pb$ (Fig. 10B), all lavas plot above the NHRL toward an enriched end member, whereas for $^{208}Pb/^{204}Pb$ versus $^{206}Pb/^{204}Pb$, the values parallel the

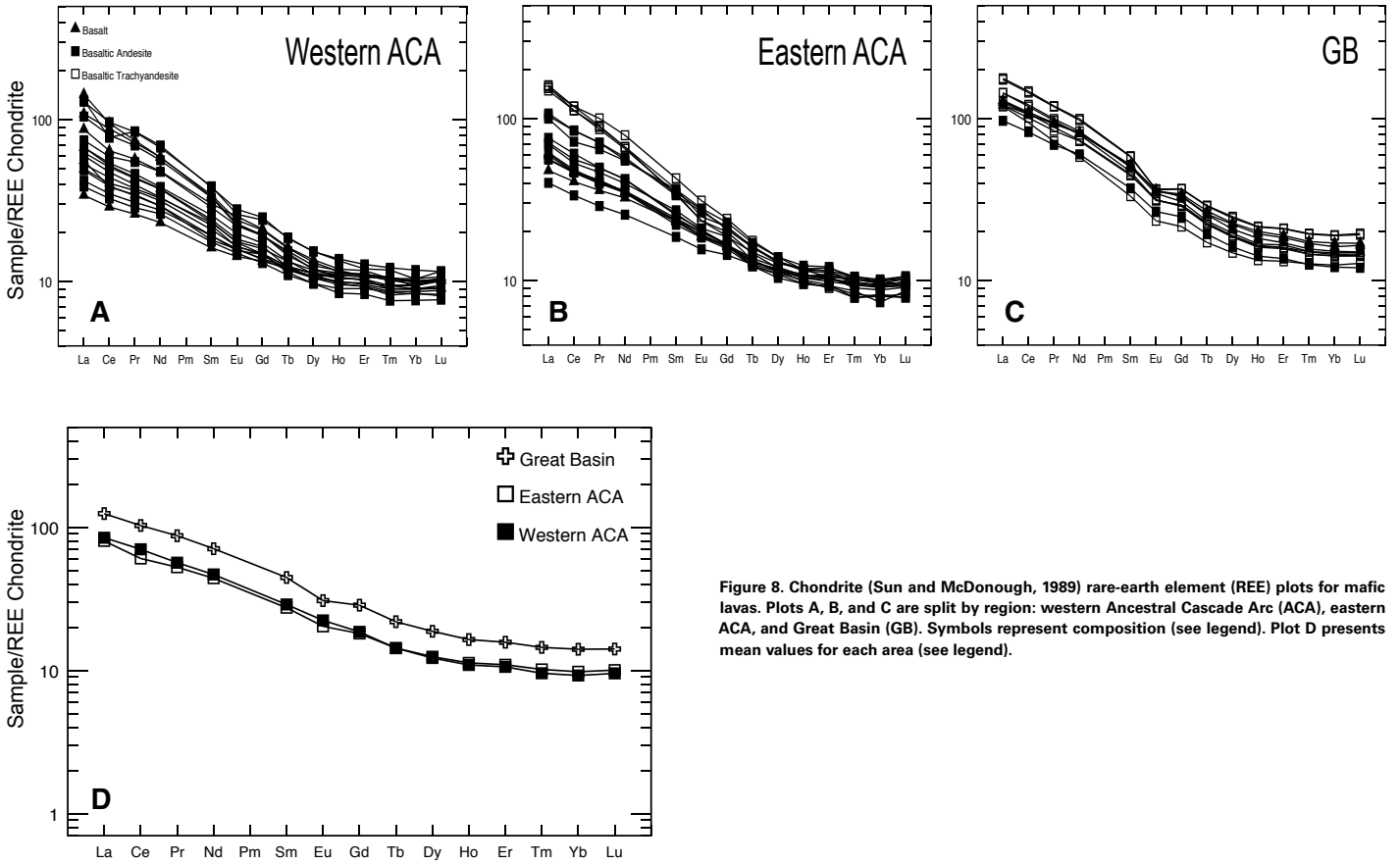

Figure 8. Chondrite (Sun and McDonough, 1989) rare-earth element (REE) plots for mafic lavas. Plots A, B, and C are split by region: western Ancestral Cascade Arc (ACA), eastern ACA, and Great Basin (GB). Symbols represent composition (see legend). Plot D presents mean values for each area (see legend).

NHRL trending toward a mantle component with high μ ($^{238}U/^{204}Pb$) and high Th/Pb (Fig. 10C). The GB mafic lavas commonly have lower $^{207}Pb/^{204}Pb$ and $^{208}Pb/^{204}Pb$ values than the ACA mafic lavas.

Figures 10D and 10E show that $^{206}Pb/^{204}Pb$ correlates with Sr and Nd isotope ratios. Comparing $^{206}Pb/^{204}Pb$ versus $^{87}Sr/^{86}Sr$ (Fig. 10D), the westernmost part of the ACA and GB lavas plot in separate clusters, and all lavas trend toward an enriched component in terms of higher Rb/Sr and μ ($^{238}U/^{204}Pb$) compared to undifferentiated material. Lavas in the westernmost part of the ACA have lower $^{87}Sr/^{86}Sr$ given their $^{143}Nd/^{144}Nd$ and $^{206}Pb/^{204}Pb$ values, as well as lower $^{206}Pb/^{204}Pb$ values for their given $^{207}Pb/^{204}Pb$ (not shown) values compared to the rest of the ACA lavas. Sample Towle #1 (Sawtooth) has the highest $^{206}Pb/^{204}Pb$ and $^{207}Pb/^{204}Pb$ values of 19.12 and 15.69, respectively. Looking to Figure 10E, GB lavas plot in a distinct cluster of $^{208}Pb/^{204}Pb$ versus $^{143}Nd/^{144}Nd$ values compared to ACA lavas.

DISCUSSION

The purpose of this study is to address three issues: (1) origin of magmatism in the GB compared to the ACA, (2) changes in geochemistry over space and time, and (3) subduction- versus extension-related magmatism. A geochemical model for Cenozoic mafic magmatism in southwestern North America should also explain: (1) the chemical variation as lavas decrease in age from east to west, (2) the sparse mafic magmatism within the GB and comparatively higher volumes of mafic magmatism within the western ACA, and (3) the broad variation in trace elements and isotopic ratios over space and time.

The trace-element and isotopic magmatic signatures within mafic lavas indicate variation of

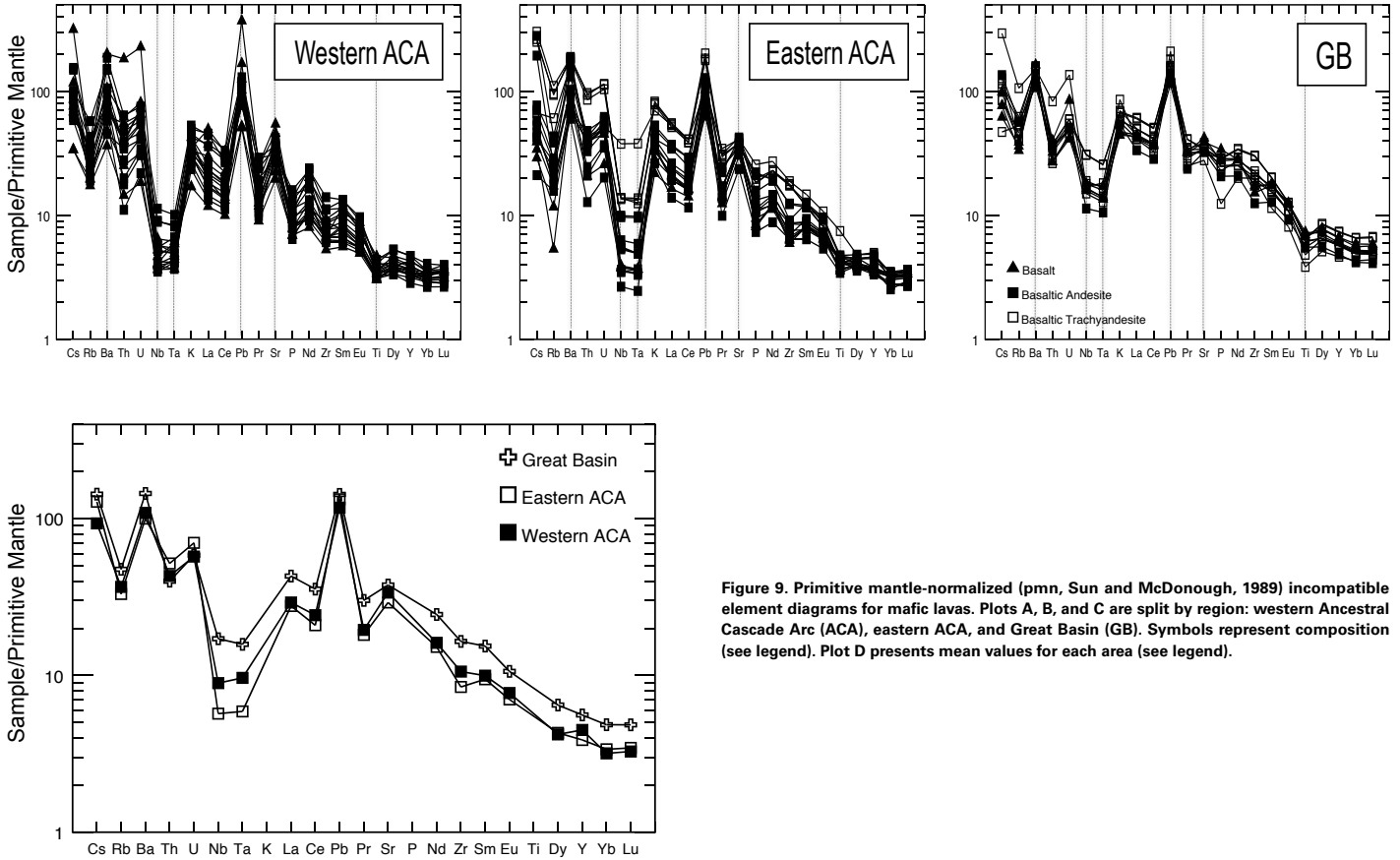

Figure 9. Primitive mantle-normalized (pmn, Sun and McDonough, 1989) incompatible element diagrams for mafic lavas. Plots A, B, and C are split by region: western Ancestral Cascade Arc (ACA), eastern ACA, and Great Basin (GB). Symbols represent composition (see legend). Plot D presents mean values for each area (see legend).

source and/or influences on the source melts. The source components in primary continental arc lavas may include: (1) depleted upper-mantle peridotite, (2) enriched mantle similar to the source of ocean-island basalt, (3) the sub-continental lithospheric mantle, (4) melt from the continental crust, (5) hydrous fluids derived from the subducting plate, (6) fluids derived from the subducting sediment, (7) partial melts of the subducting plate, and (8) partial melts of subducting sediment. Before examining source components, possible crustal contamination of the lavas after they left the source region must be addressed.

Evidence for Post-Magma Generation Crustal Contamination

Within the confines of the study area, various authors (e.g., Farmer and DePaolo, 1983, 1984) have recognized a range of different Mesozoic and Cenozoic granitoids and eugeocline sedimentary rocks, many of which are the direct or indirect product of subduction processes. Addition of these Mesozoic crustal components to mantle-derived magmas would increase the SiO_2 content and $^{87}Sr/^{86}Sr$ while lowering the Mg#, Nb/La, and $^{143}Nd/^{144}Nd$ ratios of those magmas (Brown et al., 2014). Most Sierra Nevada granitoids have high $^{87}Sr/^{86}Sr$, low $^{143}Nd/^{144}Nd$, and high $^{207}Pb/^{204}Pb$ (e.g., Barbarin et al., 1989; Cousens et al., 2008, 2009). The Sierran granitoids also have lower Ba/La and $(Sr/P)_{pmn}$ values compared to the mafic lavas. The volcanic rocks from the GB have a lower range in Mg# and higher range in SiO_2 values compared to the ACA lavas, possibly due to thicker crust during the Oligocene, when what is now the Great Basin was a high plateau resulting from Mesozoic compressive forces and crustal thickening (Henry, 2009). At the time of their eruptions, GB mafic lavas may have traveled through as much as 100 km of compositionally

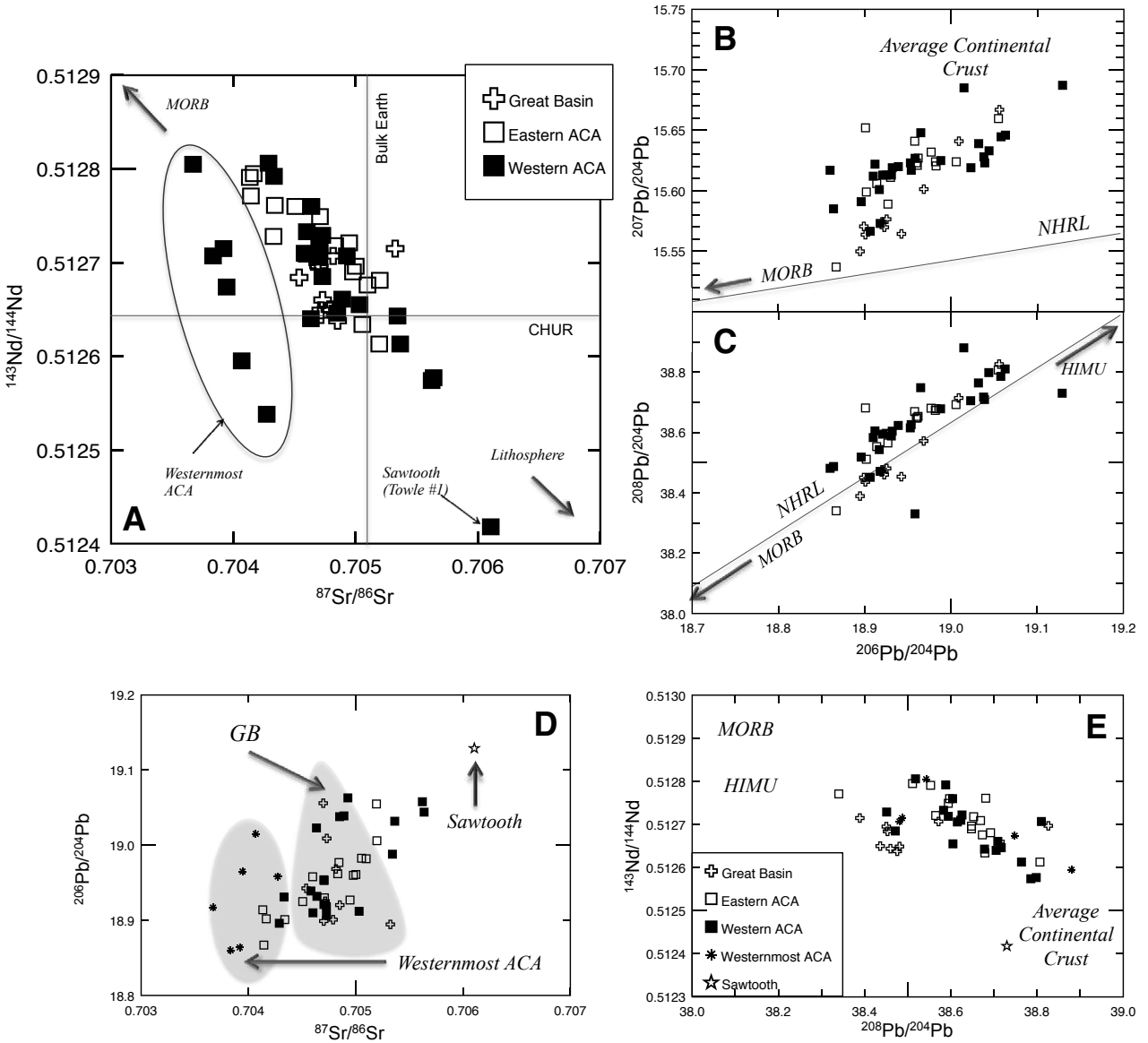

Figure 10. Plots comparing Sr, Nd, and Pb radiogenic isotopic ratios for mafic lavas (modified from Cousens et al., 2008). (A) $^{143}Nd/^{144}Nd$ versus $^{87}Sr/^{86}Sr$ graph shows a mixing line between mid-ocean ridge basalt and lithosphere end members in which CHUR is chondritic uniform reservoir (see Cousens et al., 2008, and references therein) for Great Basin (GB) and most Ancestral Cascade Arc (ACA) lavas. Lavas with lower $^{87}Sr/^{86}Sr$ values for their given $^{143}Nd/^{144}Nd$ value are referred to as westernmost ACA lavas (circled). (B) $^{207}Pb/^{204}Pb$ versus $^{206}Pb/^{204}Pb$ plot shows a trend away from the Northern Hemisphere Reference Line (NHRL) (Hart, 1984) toward the average continental crust. (C) $^{208}Pb/^{204}Pb$ versus $^{206}Pb/^{204}Pb$ plot shows lavas hovering along the NHRL toward high-μ (HIMU). (D) $^{206}Pb/^{204}Pb$ versus $^{87}Sr/^{86}Sr$ plot includes the symbols closed star as the westernmost ACA lavas (also in gray) and the open star as Sawtooth (Towle #1). GB lavas are also shown in shaded gray. (E) $^{143}Nd/^{144}Nd$ versus $^{208}Pb/^{204}Pb$ plot showing the various end members. GB lavas show lower $^{206}Pb/^{204}Pb$ values for their given $^{143}Nd/^{144}Nd$ values, perhaps due to less influence from slab-derived components.

heterogeneous continental crust compared to lesser thickened crust within the younger, western ACA lavas (Henry, 2009).

Figure 11 tests the possibility that crustal contamination of the mafic melts is a major petrological process by investigating correlations of Nb/La (Fig. 11A) and $^{143}Nd/^{144}Nd$ (Fig. 11B) with SiO_2 values. Nb/La values are low (<1) for all three regions, and both Figures 11A and 11B demonstrate no covariation with increasing SiO_2 values. The lack of correlation of Sr (Fig. 11 insert) and Nd isotopic composition with SiO_2, combined with the absence of inherited crustal quartz or zircons into the melts (determined petrographically) suggests that the isotopic and trace-element compositions of the ACA and GB mafic volcanic rocks are not strongly affected by upper-crustal contamination.

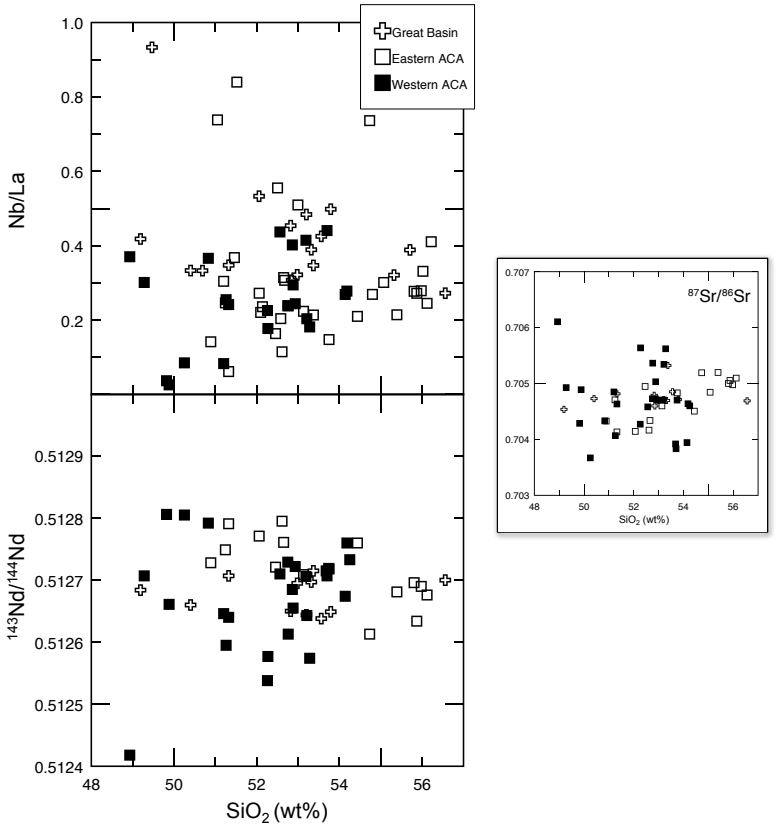

Figure 11. Crustal contamination plots: Nb/La, $^{143}Nd/^{144}Nd$, and $^{87}Sr/^{86}Sr$ versus SiO_2 wt%. See text for discussion.

High-K Magmatism and Degree of Partial Melting

Moving from east to west across the study area, mafic melts generally decrease in their K_2O, P_2O_5, TiO_2 contents and Nb/Yb (examples shown in Figs. 5A, 5D, and 12A). Mafic magmas with K_2O contents between 1%–3% are most common in the central GB. Mafic lavas from Pyramid Lake and basaltic trachyandesites from the Carson Range (eastern ACA) also show higher ranges in K_2O, P_2O_5, and TiO_2, similar to the GB mafic lavas. Ranges in Na_2O contents do not change much for GB and eastern ACA mafic lavas (2.6–4.5 wt%), slightly lower in western ACA mafic lavas (2.5–3.8 wt%), and lowest for the westernmost ACA lavas (2.1–2.6 wt%).

Major- and trace-element chemistry shown in Figures 5 (K_2O, TiO_2, P_2O_5 versus Mg#; K_2O versus SiO_2) and 12 (TiO_2 versus SiO_2, La/Sm versus La) confirms that the proportion of high-K (and shoshonitic) rocks decreases from east to west. Low degrees of partial melting of the mantle can produce melts with enriched K, Ti, and P, as well as LREE and/or HREEs. Plots involving ratios of highly incompatible elements (e.g., La and Ce) to a less incompatible element (e.g., Sm and Yb) versus the concentration of the highly incompatible element can reveal degrees of partial melting in comparison to fractional crystallization. In Figure 12B, crystal fractionation will not have a great effect on the La/Sm ratio; however, low partial melting would result in greater fractionation of La from Sm with greater La abundance, thereby providing a method for distinguishing between partial melting and crystal fractionation.

Fractional crystallization can be partially responsible for the slightly higher range in SiO_2 and lower range in Mg# for the GB mafic lavas compared to the ACA lavas; however, it cannot be the only mechanism responsible for the results seen in Figure 12. Another component is required to explain these geochemical variances for mafic lavas (i.e., with minimal range in Mg#). The chondrite-normalized REE patterns for the GB mafic lavas (Fig. 8) exhibit parallel patterns of increasing abundance with slight enrichment in LREEs relative to HREEs. The parallel REE patterns of the GB rocks imply that the mafic melts were derived from a similar mantle source region and underwent similar degrees of partial melting. The parallel REE patterns and lower Mg# values also confirm that the GB mafic melts underwent some degree of fractional crystallization before erupting at the surface. Additionally, the high LREE and incompatible trace-element contents (Fig. 9) suggest that the mantle source must have been previously metasomatically enriched

(Cousens et al., 2008). Figure 10E shows that GB lavas plot in a distinct cluster of $^{208}Pb/^{204}Pb$ versus $^{143}Nd/^{144}Nd$ values compared to ACA lavas, which also may indicate a basement (lithospheric) signature. Trace-element data indicate that melting occurred at a depth within the spinel peridotite field ($(Dy/Yb)_{pmn}$ <1.6), between 70 and 35 km (Rollinson, 2014), which dismisses the possibility of partial melts generated from garnet peridotites and/or garnet-bearing (eclogitic) subducted slab or garnet-bearing lower crust.

We can consider low degrees of partial melting (low *F*, where *F* is melt fraction) due to (1) low non-synchronous tensile stresses or faulting (Putirka and Busby, 2007; Busby and Putirka, 2009; Busby, 2013) and (2) a function of temperature and water (volatile) content released into the mantle source by the subducted slab. High K_2O volcanism is represented within the older lavas from the GB (age >14 Ma) and lavas from some regions within the eastern ACA (age <14 Ma) (Pyramid Lake and Carson Range). These high-K_2O lavas are also enriched in TiO_2, Na_2O, and P_2O_5 at Mg# between 0.45 and 0.65 for GB mafic lavas and 0.58–0.72 for Pyramid mafic lavas (Figs. 5 and 12). This observation may signify differences in the petrogenesis of lavas from these two regions. The high-K mafic lavas from the GB erupted during the initial stages of slab rollback after >30 m.y. of flat-slab subduction. The low angle between the slab and overlying CLM would result in low temperatures and therefore lower volatile release from the slab compared to the "normal" arc system (e.g., Pearce and Parkinson, 1993). In summary, the high-K_2O, TiO_2, Na_2O, and P_2O_5 lavas are due to either source-region enrichments or to low degrees of partial melting.

The <14 Ma mafic lavas from Pyramid Lake erupted near the north-south–trending Pyramid Lake fault (PLF), which formed during development of the Walker Lane (see figure 3B from Faulds et al., 2005). Although the exact age of the PLF is debated, it has been determined that the PLF has accommodated ~10 km of dextral offset during the past 9 m.y. (Faulds et al., 2005) indicating a region under considerable tensile stress since before 9 Ma. The generation and composition of the Pyramid

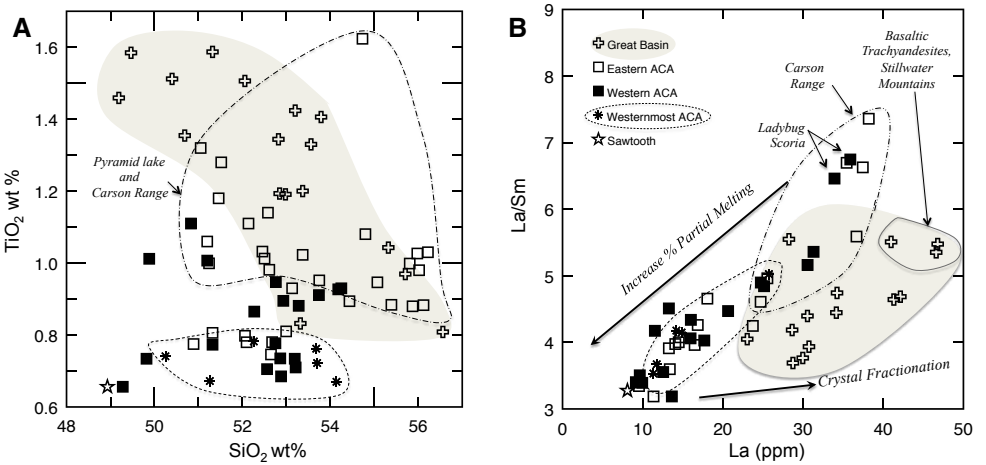

Figure 12. Partial melt diagrams that include (A) TiO_2 versus SiO_2 wt% and (B) La/Sm versus La. The field confined by the broken dashed line contains mafic lavas from Carson Range and Pyramid Lake. Diagram B includes only data from Carson Range because Sm data from Pyramid Lake is unavailable (minimal trace element data for Pyramid Lake was acquired by personal commun. from C. Henry, Nevada Bureau of Mines, 2005). Great Basin (GB) mafic lavas are shaded and westernmost Ancestral Cascade Arc (ACA) mafic lavas are circled. Mafic lava from Sawtooth (sample Towle #1) is recognized by a star. See text for further discussion.

mafic lavas are consistent with the idea that tensile stresses in the Walker Lane favored eruption of low melt fraction magmas (Takada, 1994; Putirka and Busby, 2007). The 25–15 Ma GB lavas, however, were erupted in regions that were not heavily faulted at the time of emplacement. Great Basin mafic lavas have lower Ba/Nb and Pb isotopic ratios compared to Pyramid Lake mafic lavas, and so it is suggested that the GB mafic lavas were generated under less hydrous, lower P-T conditions during the early phases of the slab rollback.

Basaltic trachyandesites from the Stillwater Mountains do not show the same partial melting trend as the other central GB mafic lavas. These GB basaltic trachyandesites show a lower-*F* melting percentage (Fig. 12B), as well as similar chemical behaviors as post-ACA lavas (Ormerod, 1988; Cousens et al., 2011) that are proposed to be generated from the lithospheric mantle: higher $^{87}Sr/^{86}Sr$ (>0.705) and $K_2O + Na_2O$ (>5 wt%). Ormerod (1988) and Cousens et al. (2011) suggested that basalts with these chemical signatures imply melting (possibly exclusively) within the CLM. It is therefore suggested that basaltic trachyandesites from the central GB formed with a major melt component from the CLM.

Chemical Contributions from Source Components

Variations over Space and Time

It is proposed that flat-slab subduction of the Farallon plate hydrated the North American CLM, perhaps as far east as the Rocky Mountains (Smith et al., 1999; Humphreys et al., 2003; Smith et al., 2004; Lee, 2005). Unlike chemical contributions from a dehydrating slab (primarily LILEs such as Rb, Ba, and Sr), the CLM adds a wider range of its trace-element content to the melt (Ce, Sm, P, Ta, Nb, Zr, Hf, Ti, Y, and Yb). Lee et al. (2001) and Kempton et al. (1991) suggested that the CLM is enriched in Mg and Ni compared to the continental crust and is also enriched in LREEs compared to the primitive mantle. Also, melts from the CLM have low $^{143}Nd/^{144}Nd$ and variable $^{87}Sr/^{86}Sr$ compositions compared to the asthenosphere due to metasomatism

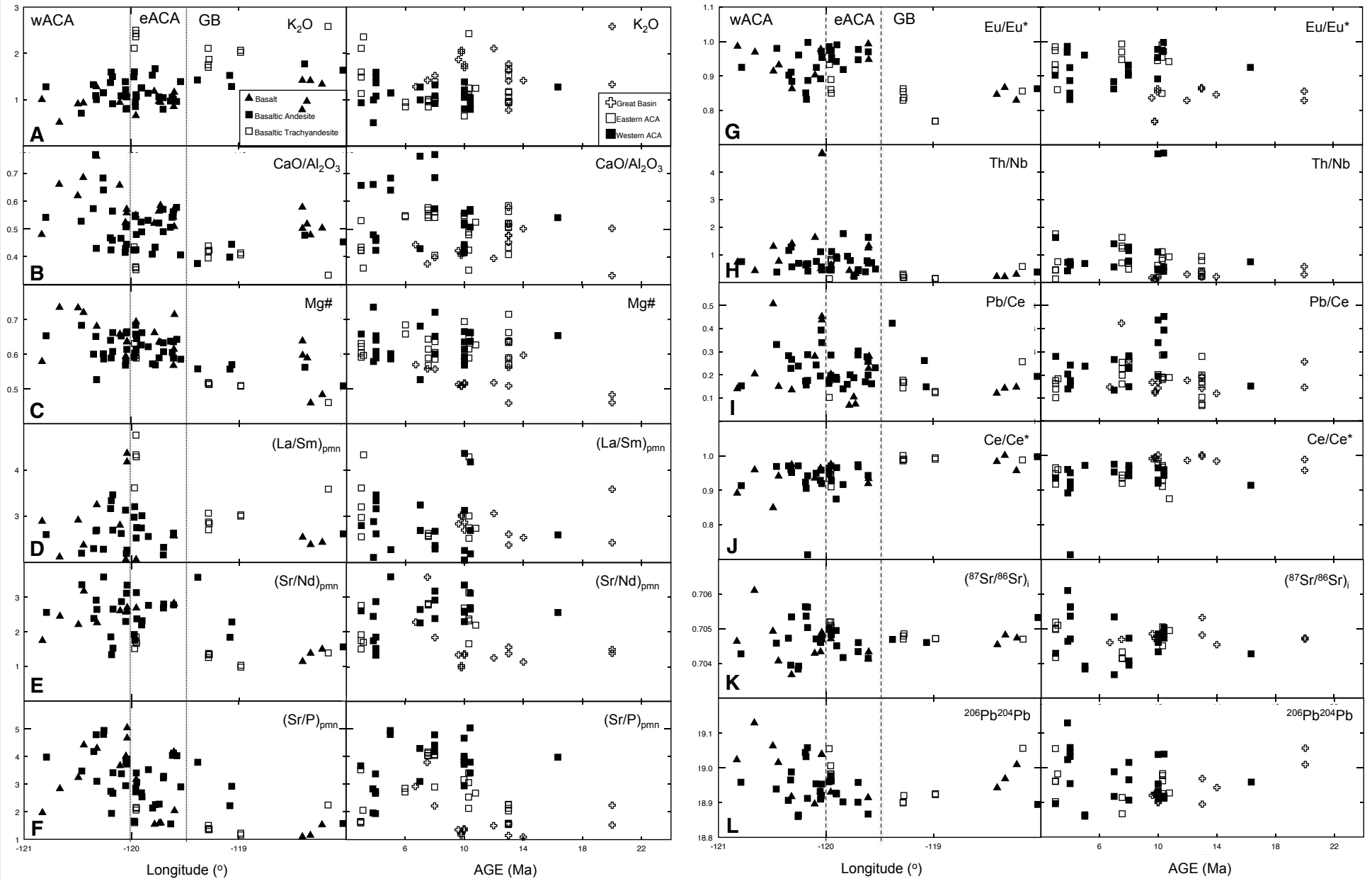

Figure 13. Diagrams evaluating major, trace and isotopic data trends over distance (longitude) and time (age). Note that the data symbols presented in the left column represent composition, whereas the symbols presented in the right column represent the three major locations (see legend). See text for discussion.

and the age of the lithospheric mantle (e.g., Omerod, 1988; Omerod et al., 1988; Cousens et al., 2008). Figure 13 presents major, trace, and isotopic data trends along the east-west transect (left column) and as a function of age (right column). Note that the data symbols in the left column represent composition, whereas symbols in the right column represent location. Figure 13 explores assimilation within the deeper crust (Fig. 13A, K_2O) and fractional crystallization (Fig. 13B, CaO/Al_2O_3), both of which have higher values in the basaltic trachyandesites of the GB and some eastern ACA lavas (Carson Range) compared to other lavas from the area. Mafic lavas show a slight increase in Mg# (Fig. 13C) from east to west, and all three rock types overlap. $(La/Sm)_{pmn}$ values vary between 2.0 and 3.5 with distance and time, showing abrupt peaks at longitude 120° and at ages 12 Ma and 3 Ma (Carson Range) (Fig. 13D). This pattern is mirrored by La/Yb and Cs/Rb (not shown), with the highest values in scoria for Ladybug Peak and Carson Range basaltic trachyandesites ($(La/Sm)_{pmn} > 4$ for samples 01-LT-46–48). The sum of REEs (not shown) and the depth of negative Eu/Eu* anomalies steadily decrease from east to west, whereas $(Sr/Nd)_{pmn}$ and $(Sr/P)_{pmn}$ values increase from east to west as well as from oldest to youngest (Figs. 13E–13G). LILE and/or HFSE values also increase to the west and with younger age. Figures 13H–13J show proxies for sediment melts, represented by Th/Nb, Pb/Ce, and Ce/Ce* ratios. The presence of sediments can affect these ratios; for example, Th/Nb and Pb/Ce are considerably higher in sediments (e.g., Pb/Ce > 0.3) compared to more uniform values for a MORB-like mantle (e.g., Pb/Ce < 0.04, White, 2013). In a similar manner, sediments may inherit seawater's negative Ce/Ce* anomaly (Class and le Roex, 2008). Under low P-T conditions, neither Th nor Nb are particularly soluble in slab aqueous fluids; however, under higher P-T conditions, subducted sediment will melt, releasing Th into the mantle wedge, while Nb remains within the sediment residue (Pearce and Peate, 1995). Therefore, fractionation between Th and Nb results from the assimilation of sediment melts in an arc system (Johnson and Plank, 1999; White, 2013). The Th/Nb and Ce/Ce* data show that the sediment signature in the mafic lavas increases from east to west. An example of radiogenic isotopic variation is shown in Figures 13K and 13L: initial Sr and Nd (not shown) isotopic ratios have a more restricted range in values toward the east end of the study area compared to the larger variation in values to the west. Lead isotopic ratios show the highest variation in central GB mafic lavas as well as toward the western ACA lavas, compared to very little variation in westernmost GB lavas.

Depth of Melting

Since heavy REEs and Y are compatible in garnet, partial melts of a garnet-bearing source (i.e., garnet peridotite or eclogite) should have high middle and/or heavy REE ratios relative to melts of spinel peridotite. With the exception of one sample from Carson Range ($(Dy/Yb)_{pmn} = 1.6$), the $(Dy/Yb)_{pmn}$ ratios for the mafic lavas from all regions are <1.5, supporting a garnet-free source (George et al., 2003). Also considering geochemical evidence of a plagioclase-free source (absence of strong Eu anomaly and high Al_2O_3 and Sr values), it can be concluded that the mafic magmas originated at a depth within the P-T conditions for spinel-peridotite (35 and 70 km, Kinzler, 1997).

Contributions from the Slab

Aqueous fluid-mobile elements, such as Cs, Sr, Rb, Ba, Pb, and U, would be released from the dehydrating slab (basalt and sediments) into the overlying mantle, increasing their abundance in the mantle compared to the HFSE and the REE. Therefore, aqueous fluid transport should result in higher ratios of Ba to Th, Pb to Ce, and Sr to Nd.

In contrast, enrichments in "fluid-immobile" Th relative to a less mobile element (HFSEs, e.g., Th/Nb) can be attributed to a partial melt of subducted sediment (e.g., Plank and Langmuir, 1988, 1993, 1998; Elliott et al., 1997; Hawkesworth et al., 1997; Johnson and Plank, 1999; Elliott, 2003) along with negative Ce/Ce* anomalies and isotopic characteristics of $^{87}Sr/^{86}Sr$ (up to 0.7060) and $^{143}Nd/^{144}Nd$ (as low as 0.51270). Figures 14A and 14B (as well as Figs. 13H and 13J) show less influence from slab fluids and the sediment component to be absent in the east and in older rocks (GB mafic lavas),

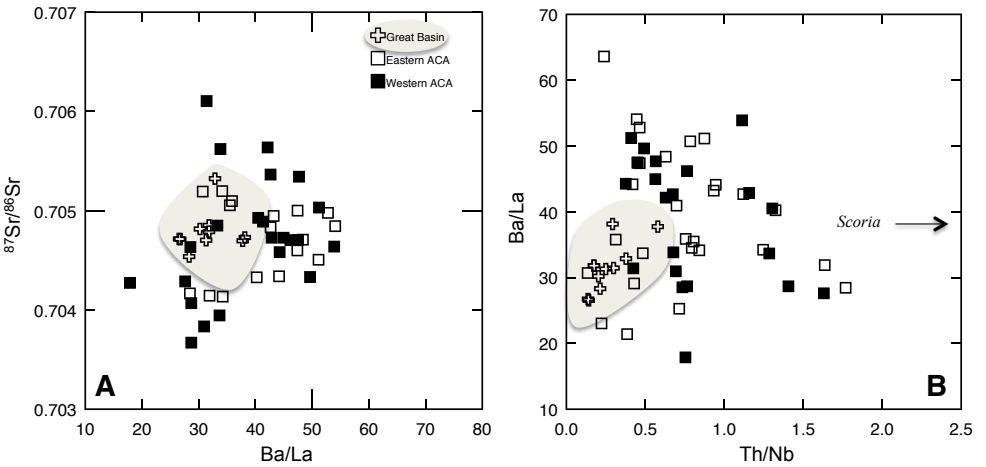

Figure 14. Isotope and trace-element ratio plots that can show influence from the source melts; specifically, fluid mobile elements from slab-derived aqueous fluids (Ba, Sr), fluid "immobile" elements from slab-derived sediment (Th) and/or in the continental lithospheric mantle (CLM) ($(^{87}Sr/^{86}Sr)_i$). A) $^{87}Sr/^{86}Sr$ versus Ba/La, B) Ba/La versus Th/Nb. Arrow indicates values for Ladybug scoria trend to Th/Nb = 4.7. Please refer to the text for further discussion.

whereas higher influence from slab fluid and a minor sediment signature is present for the ACA lavas. The sediment signature occurs at 120° longitude at ca. 10–12 Ma, which may indicate either P-T conditions were more favorable for sediment melting (>800 °C at 3 GPa, Nichols et al., 1994; Johnson and Plank, 1999) or that more sediment was present on the slab surface.

Involvement of sediment in subduction-related melts may also have had an influence on the $^{207}Pb/^{204}Pb$ and $^{208}Pb/^{204}Pb$ ratios. Components from subducted oceanic sediments can emerge in arc volcanic rocks in the form of chemical tracers (e.g., Johnson and Plank, 1999; Kessel et al., 2005). Ocean sediment is chemically variable from a composition that includes volcaniclastic deposits, chert, silt, biogenic deposits, clay, continental discharge, and interstitial seawater (Church, 1976; Lackschewitz et al., 2000; Kessel et al., 2005; Prytulak et al., 2006). In continental subduction zones, seafloor sediments are either scraped off the subducting plate at the ocean trench and accreted along the continental plate margin or subducted along with the oceanic plate; as a result, they contribute to arc magmatism and/or are recycled in the convecting mantle (Plank and Langmuir, 1993). Melts from subducted sediments should leave a chemical signature in the erupted arc lavas; however, the bulk chemical composition of the original sediments needs to be determined. The terrigenous sediments that have been scraped off along the Coast Range in California and accreted as metasediments are >100 m.y. old (Wakabayashi, 1992) and therefore are too old to be associated with the Cenozoic magmatism. We therefore compare our geochemical data to the bulk compositions of sediments from modern subduction environments, namely drill core acquired from the Gorda plate, which is located off the coast of northern California. Sediments recovered from the Escanaba Trough, the southernmost point of the Gorda plate, are olive-green to gray hemipelagic silty clay. Bulk chemical analyses, including trace elements (Th, Ce, and Nb, Lackschewitz et al., 2000) as well as radiogenic isotopic compositions (Prytulak et al., 2006) are plotted in the graphs presented in Figure 15.

Trace-element and isotopic tracers for sediment melts in arc volcanic rocks include Th and Pb (Plank and Langmuir, 1992, 1993; Hawkesworth et al., 1997), which can be presented as high Th/Nb, $^{207}Pb/^{204}Pb$, and $^{208}Pb/^{204}Pb$ ratios. Lead and Th can once again become mobilized within sediment melts (Plank and Langmuir, 1992; Hawkesworth et al., 1997).

Figures 10B and 10C show that all samples have elevated Pb isotopic ratios compared to MORB and plot above (Fig. 10B) or along (Fig. 10C) the NHRL (Hart, 1984). The GB mafic lavas have slightly lower $^{207}Pb/^{204}Pb$ and $^{208}Pb/^{204}Pb$ and plot closer to the NHRL than the western ACA lavas, perhaps due to lower Pb input from the slab and less recycled crustal Pb in the mantle farther away from the plate margin. Figures 10D and 10E compare $^{206}Pb/^{204}Pb$ to $^{87}Sr/^{86}Sr$ and $^{143}Nd/^{144}Nd$, respectively. Combined with the Ce/Ce* data, the ACA mafic lavas that trend to higher $^{206}Pb/^{204}Pb$ at equal $^{143}Nd/^{144}Nd$ values are consistent with more sediment in the ACA mantle source.

All mafic lavas have variable Sr and Nd isotope compositions (Fig. 10). The degree of variation

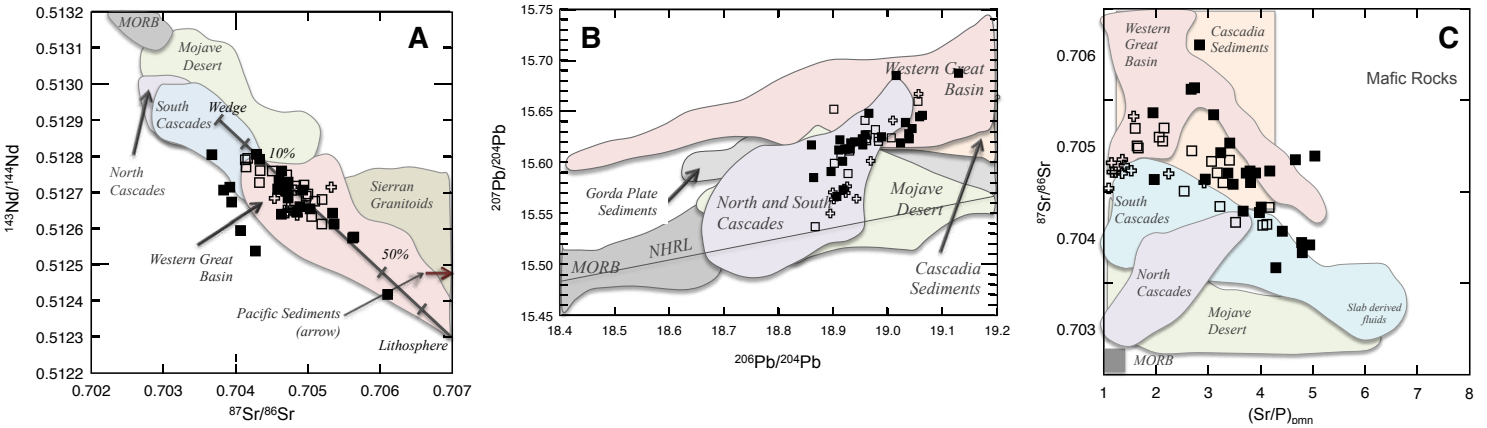

Figure 15. (A) and (B) Sr-Nd and Pb isotopic plot, and (C) $^{87}Sr/^{86}Sr$ versus $(Sr/P)_{pmn}$ (primitive mantle normalized), comparing mafic lavas from the study area to fields for the Gorda Ridge mid-ocean ridge basalts (MORBs, Davis and Clague 1987), Mojave Desert and the western Great Basin (GEOROC, 2007), and the Sierran granitic rocks. The data on Gorda basin sediments are taken from Church (1976) and Church and Tilton (1973). The Sr-Nd isotopic values for Pacific sediments are outside the graph with whole-rock values averaging $^{87}Sr/^{86}Sr = 0.7091$ and $^{143}Nd/^{144}Nd = 0.5124$ (Goldstein and O'Nions, 1981). Mixing curve is for melts of lithosphere (Sr = 1200 ppm, Nd = 38 ppm, $^{87}Sr/^{86}Sr = 0.7070$, $^{143}Nd/^{144}Nd = 0.5123$) and melts of mantle wedge (Sr = 550 ppm, Nd = 15 ppm, $^{87}Sr/^{86}Sr = 0.7038$, $^{143}Nd/^{144}Nd = 0.5129$) with tick marks showing percentage of lithospheric melt in the mix (modified from Cousens et al., 2008, and Yogodzinski et al., 1996). The Northern Hemisphere Reference Line (NHRL) is from Hart (1984) and based on Pb isotopic values from MORB and ocean-island basalt (OIB). The data on Gorda basin sediments are taken from Church (1976) and Church and Tilton (1973). Cascadia sediments are from Davis et al. (1998) and Prytulak et al. (2006). Great Basin lavas represented by open crosses; eastern Ancestral Cascade Arc (ACA) lavas represented by open squares; western ACA lavas represented by filled squares.

increases from east to west, with the greatest variation occurring in mafic lavas from the eastern and western ACA. Figure 15 compares the Sr, Nd, and Pb isotopic data from this study with data from several neighboring physiographic regions summarized in Cousens et al. (2008). All lavas shift away from the MORB field and trend toward an isotopically enriched source. In Figure 15A, most mafic lavas from all locations plot along a mixing line between the modern south Cascade arc mantle wedge and the enriched CLM that is a typical source for alkali basalts in the western Great Basin (Menzies et al., 1983; Ormerod et al., 1991). Mafic lavas from the westernmost part of the ACA, however, plot to the left of the array, with lower Sr isotopic ratios compared to other lavas with a given $^{143}Nd/^{144}Nd$. Sources of higher $^{87}Sr/^{86}Sr$ include seawater, subducted sediments, upper continental crust, and metasomatized CLM. If higher $^{87}Sr/^{86}Sr$ within the other ACA and GB lavas is derived from mixing with the metasomatized CLM (Fig. 15A), the lower $^{87}Sr/^{86}Sr$ values in westernmost ACA lavas could be attributed to (1) the absence of or presence of a chemically different metasomatized CLM, (2) melt generation deeper in the mantle wedge, or (3) mixing with crustal terrane distinct from the CLM. The westernmost ACA mafic lavas also show lower La/Sm and Pb/Ce values. The north-south–trending CLM under the westernmost ACA is possibly older and less enriched in LILE and LREE elements, including Sr.

Earlier, it was noted that high abundances of LILE and LREE and low abundances of HFSE in lavas erupted in an arc system can be attributed to involvement of fluids transported into the mantle wedge from the subducted slab (Hughes, 1990; Leeman et al., 1990; Baker et al., 1994; Borg et al., 1997). Similarly, by confirming correlation between $((Sr/P)_{pmn}$ and $(Sr/LREE)_{pmn}$, previous workers have used higher $(Sr/P)_{pmn}$ values as a proxy for slab-derived components in the mantle wedge (Borg et al., 1997). We can compare the results from the GB and ACA lavas to neighboring provinces presented in Borg et al. (1997) and Cousens et al. (2008). Figure 15C shows the variation in Sr relative to P (used to reflect variation in Sr-rich slab-derived fluids added to the mantle wedge) at a given $^{87}Sr/^{86}Sr$ for mafic rocks compared to other regions in the western United States. Increases in $(Sr/P)_{pmn}$ for mafic lavas from the western ACA, from Lousetown and sample 01-LT-53 from the Carson Range, are consistent with higher slab fluid content of mantle sources overlying the subducted slab. The $(Sr/P)_{pmn}$ values from the eastern ACA samples show a negative correlation with $^{87}Sr/^{86}Sr$. Mafic lavas from the GB have very low $(Sr/P)_{pmn}$ values compared to other regions but have $^{87}Sr/^{86}Sr$ that are elevated compared to all other nearby magmatic suites with the exception of the western Great Basin. To the west, $(Sr/P)_{pmn}$ values increase indicating an increasing contribution from slab fluids to the mantle source, which is consistent with trace-element patterns shown in Figures 9 and 13. For example, the trend in Ba/Nb (not shown) suggests that, although all lavas show influence from the subducted Farallon slab, the subduction signature increases from east (older) to west (younger). The similarities in phenocryst compositions, REE, and isotopic signatures amongst the GB mafic compositions further support the derivation of their primary magmas from similar source regions, with variations in chemistry due to a range of contributions from the CLM and variable degrees of partial melting (*F*). We can conclude that the mafic lavas that erupted within the GB were generated within drier, low P-T conditions compared to the mafic ACA lavas. The western ACA mafic lavas were generated within highest P-T conditions with the highest slab fluid content compared to eastern ACA and GB lavas. The P-T conditions and volatile content relate to the degree of slab dip; that is, shallow dip would result in lower P-T conditions and less dehydration of the slab. A larger subduction angle would result in higher P-T conditions and greater dehydration, releasing more fluids (Ba, Rb, Sr, and La). Then, as the slab continues to descend, sediment melts and contributes a component to the mantle wedge. Pressure-temperatures conditions were not high enough to melt the basaltic slab itself, therefore retaining the HSFE (Nb and Ta).

The 0.706 Line

The $^{87}Sr/^{86}Sr = 0.706$ isopleth (where $^{87}Sr/^{86}Sr$ is the initial Sr-isotope ratio of plutonic rocks) defined by Kistler and Peterman (1973, 1978), commonly known as the 0.706 line, has been interpreted to mark the transition from Precambrian continentally derived rocks on the east to Phanerozoic volcanic arc–derived rocks on the west (Kistler and Peterman, 1973, 1978; Farmer and DePaolo, 1983; Elison et al., 1990). Kistler and Peterman (1973) interpreted the 0.706 line as the western edge of the Precambrian crystalline basement (Fig. 1). The 0.706 line is recognized in Mesozoic and younger igneous granitoid rocks from western North America (Kistler, 1990) and Cenozoic volcanic rocks, as noted by Kistler and Peterman (1973).

The correlation of chemical characteristics in Cenozoic basalts from this study with their proximity to the 0.706 line (Reid and Ramos, 1996) implies that they are at least partially derived from the CLM (Kempton et al., 1991; Reid and Ramos, 1996). Figure 1 includes the 0.706 line (heavy dashed line) taken from Kistler (1990) and confirms that the sampled mafic lavas mostly lie to the west of the 0.706 line with one exception of a 3.82 Ma basalt from Sawtooth Ridge (sample Towle #1, SiO_2 = 48.93 wt%, Mg# = 0.74), which has an $^{87}Sr/^{86}Sr$ value >0.706, and $^{143}Nd/^{144}Nd$ value <0.5125.

Subduction- versus Extension-Related Magmatism

Between 35 and 3 Ma, arc volcanism migrated southwestward across what is now the Great Basin. At ca. 17 Ma, Great Basin extension began (Colgan et al., 2006a, 2006b); thus, any volcanic rock in the region *younger* than 17 Ma in age may have been produced by arc processes, extension-related partial melting of the mantle, or a combination of both (Dickinson, 2006; Cousens et al., 2008; Busby and Putirka, 2009; Busby, 2012). Slab rollback completed its migration across the Great Basin by ca. 16 Ma, when the arc front reached the eastern Sierra Nevada (Busby et al., 2008; Busby and Putirka, 2009; Busby, 2013). Since the timing of both arc and extensional processes overlap, it is therefore difficult to establish by age alone which process generated ACA lavas. We have established that all mafic lavas have strong trace-element

subduction signatures, which suggest a role for a subduction-modified mantle source.

Caldera-forming magmatism, known as the "ignimbrite flare-up," dominated the GB during the magmatic sweep east of the Stillwater Range (Dickinson, 2002, 2006, 2013; Henry, 2008; Best et al., 2009), which was emplaced through >100 km thickened crust referred to as the "Nevadaplano" (DeCelles, 2004). It is possible that east of the Stillwater Range, mafic magmas would pond at depth, partially melt and assimilate lower and upper crust, and thus form a caldera field. To the west of the Stillwater Range, no calderas are present, suggesting that the lithosphere was thin enough that mafic magmas could reach the surface. Assuming that the calderas of the ignimbrite flare-up indicate the position of the continental arc over time, then the only clear expressions of younger magmatism (postarc) are the basalt, basaltic andesite to basaltic trachyandesites of the Stillwater Range (La Plata Canyon, southwestern range margin). Calderas of the southern Stillwater Range are ca. 29–25 Ma in age (Hudson et al., 2000; Henry and John, 2013), but the Stillwater basaltic rocks are 15–14 Ma in age, ~10 m.y. younger than the caldera events. We infer that extension reached the Stillwater Range at ca. 15 Ma, when normal faulting may have allowed mafic magmas to reach the surface. A backarc origin, however, cannot be discounted. We can compare the ca. 15 Ma mafic rocks from Stillwater Range to other known postarc extension-related mafic lavas from small volcanic fields in the Reno-Fallon area (Cousens et al., 2012) and from the Owens Valley (e.g., Big Pine volcanic field, Fig. 16). Stillwater mafic rocks have primitive mantle-normalized incompatible element patterns very similar to the average for other GB mafic lavas, all having a subduction signature. The Stillwater lavas are also similar to extension-related subalkaline basalts from the Big Pine volcanic field in the Owens Valley, where Great Basin extension is proposed to melt metasomatized lithospheric mantle (Ormerod et al., 1991). The average pattern for lava blocks from Upsal Hogback volcano near Fallon, an example of postarc volcanic rocks in western Nevada, has lower Ba/La, La/Nb, and a more within-plate trace-element composition compared to GB volcanic rocks. We conclude that if the Stillwater mafic lavas are extension related, then they are partial melts of the same mantle source that produced the arc-related GB mafic lavas.

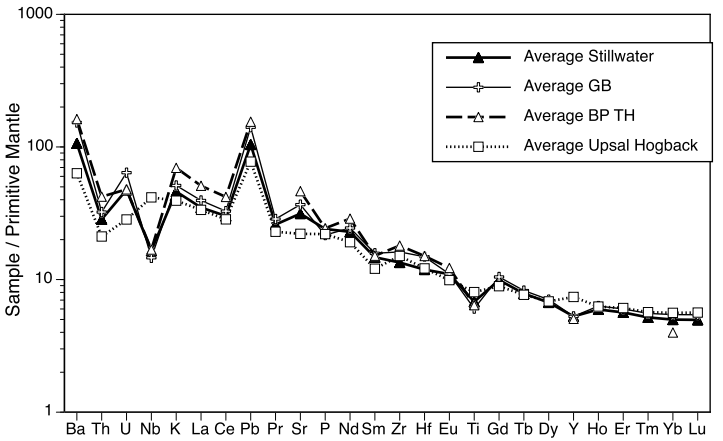

Figure 16. Average primitive mantle-normalized (values of Sun and McDonough, 1989) patterns for the averages of Miocene Stillwater mafic lavas, Great Basin (GB) mafic lavas, tholeiitic basalts from the Big Pine (BP) volcanic field (BP TH—Big Pine Tholeiites) in the Owens Valley (Ormerod et al., 1991) south of this study area, and basalt bombs from Upsal Hogback volcano near Fallon (Cousens et al., 2012). The Miocene Stillwater rocks have patterns similar to arc-related GB lavas and extension-related Big Pine basalts, indicating that arc magmatism and extensional magmatism can tap sources with similar incompatible element characteristics.

Model for GB-ACA Mafic Magmatism

At 40 Ma, a high rate of convergence of the Farallon plate (10–15 cm/yr, English and Johnston, 2004) resulted in flat-slab subduction (English et al., 2003; DeCelles, 2004; Liu et al., 2008) underneath the North American plate; this subduction thickened the lithosphere and amplified the relief in the Sierra Nevada and in what is now the Great Basin (Fig. 17A) (DeCelles, 2004; Henry, 2009). The East Pacific Rise was ~200 km from the edge of the North American plate, and the thermal structure of the Farallon plate was influenced by its young age, shear heating from the flat-slab subduction (Peacock et al., 1994; Peacock, 1996), and fast subduction rate, allowing incompatible elements to be released from the slab (i.e., dehydration) and chemically enrich the overlying CLM.

Flat-slab subduction, which currently occurs in 10% of modern convergent margins (Gutscher et al., 2000b), can be caused by (1) a high rate of convergence of the overlying plate and/or (2) the buoyancy of thickened oceanic crust of moderate to young age (Gutscher et al., 2000b). In the flat-slab scenario for the Farallon plate, it has been argued that there is no asthenospheric mantle wedge between the North American lithospheric mantle and the Farallon plate (DeCelles, 2004; Liu et al., 2008). This can cause a delay in the basalt to eclogite transition by up to 8 to10 m.y. (Gutscher et al., 2000b) due to the cool thermal structure of two overlapping plates (Gutscher et al., 2000a; Arcay et al., 2007). Dehydration of metabasaltic oceanic crust directly enriches the CLM; however, no melting took place because of lack of heat. High intraplate coupling may have scraped off much of the sediments at the wedge, possibly explaining the absence of a sediment-sourced chemical signature in the GB lavas. As subduction progressed, the oceanic crust and lithospheric mantle underwent metamorphic

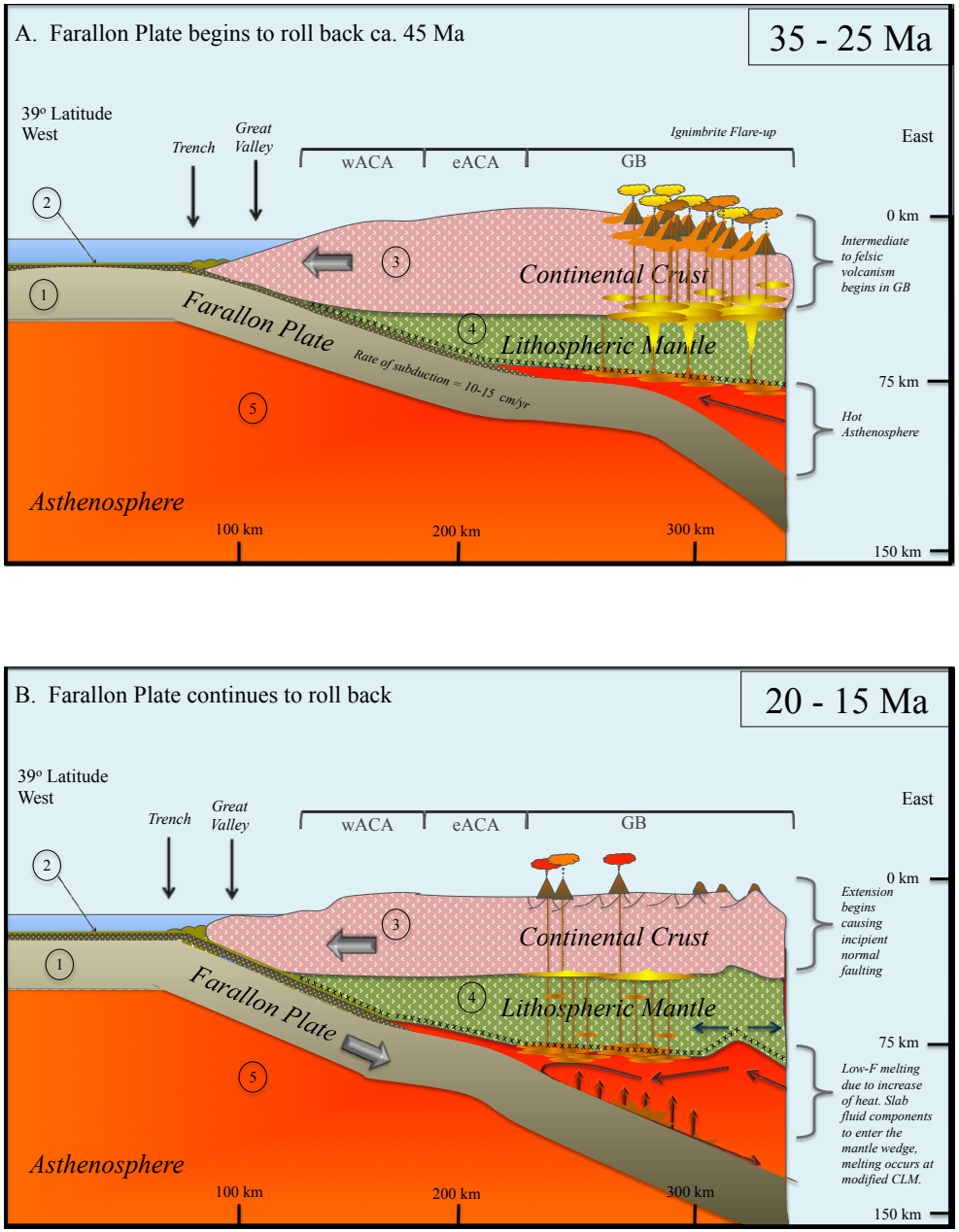

Figure 17. Model summarizing the southwestward magmatic migration within the study area (37° latitude) from 40 to 3 Ma, based on the geochemical and petrological results on mafic magmas. Circle 1 represents the meta-basaltic subducting oceanic plate; circle 2 represents slab sediment; circle 3 represents the upper and lower continental crust; circle 4 represents the continental lithospheric mantle (CLM); and circle 5 represents the convecting mantle (asthenosphere). 40 Ma: thickened crust at the western North American margin resulting from flat-slab subduction toward the end of the Laramide orogeny. The CLM is enriched in components derived from the slab (e.g., rare-earth elements [REEs], Sr, and Pb), represented by the crosses located along the lower boundary of the lithospheric mantle. (A) From 35 to 25 Ma, the Farallon slab begins to roll back increasing heat into the system from the asthenosphere. Possible basaltic underplating and assimilation fractional crystallization processes resulted in violent volcanic eruptions, signifying the "ignimbrite flare-up" as presented in Henry and John 2013 (and references therein). (B) By 20–15 Ma, high-K intermediate and mafic magmatism in central Great Basin (GB) migrated southwestward as the Farallon plate continued to roll back, and extension reached the Stillwater Range at ca. 15 Ma, when normal faulting may have allowed mafic magmas to reach the surface. (*Continued on following page.*)

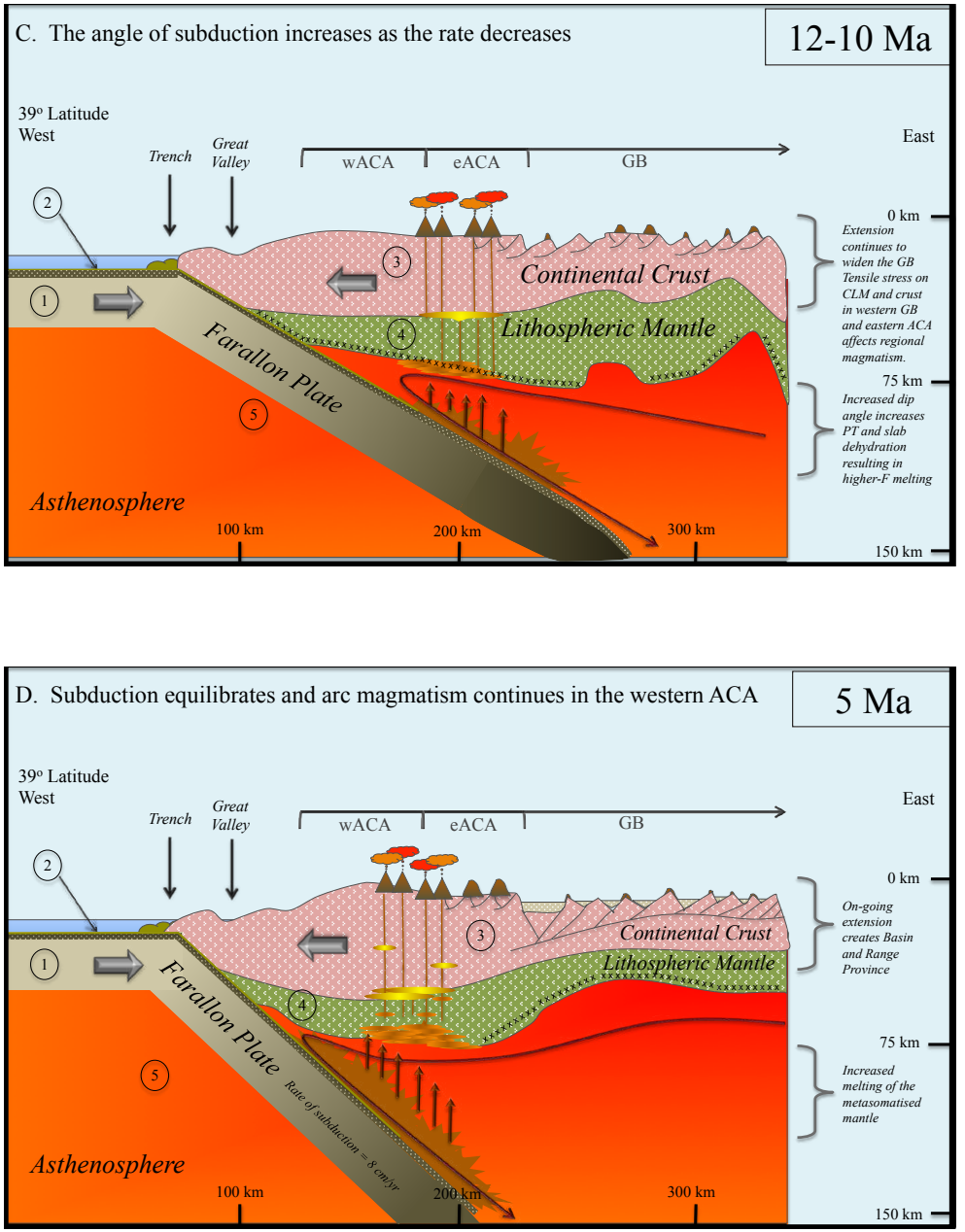

Figure 17 (*continued*). (C) Circa 12–10 Ma extension related faulting in the western GB and selected eastern Ancestral Cascade Arc (ACA) regions (e.g., Pyramid Lake) altered the chemistry of the resultant melts. Intermediate to mafic magmatism continued in the eastern and western ACA. PT—Pressure and Temperature. (D) By 5 Ma, Farallon slab has equilibrated in the western ACA, and arc magmatism is established in the Sierra Nevada (western ACA). Please refer to the text for a more detailed discussion.

transformation far into the North American plate, which would have increased the density of the subducted slab. As the hydrous minerals continued to break down, they would have released substantial amounts of H_2O and other fluid-mobile elements into the CLM, thereby altering the rheological properties of the boundary between the slab and CLM, which would have reduced the intraplate coupling above a flat-slab segment (Gutscher et al., 2000a). The density of the slab probably increased by up to 10% once the basalt was transformed to eclogite, causing the lithospheric plate to sink at a steeper angle, at which point slab detachment from the base of the North American plate was possible (Spencer et al., 1995).

As the convergence rate between the Farallon and North American plates decreased, the density of the metamorphosed (eclogitic) slab increased, and the slab hinge point started to roll back (Fig. 17B). As the slab hinge point rolled back, hot asthenosphere likely moved in between the North American and subducted Farallon plates, initiating dehydration of the slab and triggering partial melting (*F*) of the hydrated CLM and the mantle wedge at the CLM boundary. Low-*F* mafic melts of the GB were generated within the spinel field of the mantle, enriched in incompatible elements including the REEs, K, P, Ti, and HFSEs. Magmatism migrated southwestward as the Farallon slab hinge point continued to roll back (Fig. 17C), and high-K lavas of Bell Canyon, Stillwater, Truckee Range, and Hot Springs Mountain erupted in the GB at ca. 25–15 Ma. The similarities in phenocryst compositions, REE, and isotopic signatures amongst GB mafic compositions further support the derivation of their primary magmas from similar source regions, with variations in chemistry due to a wide range of contributions from the CLM and mantle wedge and variable degrees of partial melting (*F*). Alkaline melts (basaltic trachyandesites) within the GB represents melting primarily in the CLM.

To the southwest, the Pacific plate margin collided with the North American plate at ~34° latitude at ca. 25 Ma, initiating a right-lateral strike-slip fault near the present site of Los Angeles (Schellart et al., 2010), creating the MTJ that began migrating northward relative to stable North America at ~33 mm/yr (Atwater and Stock, 1998). Intermediate volcanism migrated southwestward across Nevada as the Farallon plate hinge point rolled back and dipped more steeply into the mantle, increasing P, T, and resultant dehydration (aqueous fluid) from the slab. Extensional and transtensional stresses likely aided the upward movement of mafic magmas starting at ca. 15 Ma within what is now identified as the Walker Lane. By 12–10 Ma, the rate of subduction slowed as well as the rate of east-west migration, and higher volumes of mafic magmatism erupted in the eastern ACA (Fig. 17D). As the angle of subduction increased, heating of the slab resulted in larger contributions from the slab-derived fluids into the widening mantle wedge. Concurrently, the slab window was expanding to the south of the study area (latitude ~31°) as the MTJ continued to migrate northward (Atwater and Stock, 1998; Schellart et al., 2010) at a rate of ~52 mm/yr (Atwater and Stock, 1998). Extension continued to fracture and thin the lithosphere in the northern and southern Basin and Range (Dickinson, 2002; Henry, 2009; Schellart et al., 2010) as well as to increase the lithospheric transtensional stress between eastern ACA and western GB (from Sparks, around Pyramid Lake, Lousetown, Coal Valley, and Carson Range). The angle of subduction increased west of longitude 120°, and P-T conditions at the slab-mantle wedge interface were high enough to allow sediment melt components from the Farallon slab to infiltrate the mantle wedge. By 5 Ma, the rate of subduction slowed to 8 cm/yr (English and Johnston, 2004), and the slab dip angle equilibrated in the mantle (Fig. 17E). Slab components continued to infiltrate the mantle wedge ($(Sr/P)_{pmn}$ = 2–5), and melting resulted in mafic extrusives in the western ACA (Stampede Reservoir, Ladybug region, Portola, and Mount Lincoln). Up to this point, arc magmatism in the entire ACA shared the same two mantle sources (lithospheric mantle and mantle wedge), thus emplacement in extended versus unextended terrane had no influence on geochemistry. Farther to the west, however, a distinct, less enriched lithospheric mantle component may have contributed to magmas in the westernmost part of the ACA (Sierra Nevada, including lavas of Squaw Peak, Pond Terrace, Devil's Peak, and Lowell Ridge), resulting in overall lower $^{87}Sr/^{86}Sr$ isotopic ratios. The mafic melt generated at Sawtooth (3.82 Ma) may have been derived from or mixed with an older, more enriched mantle source mixed with a component possessing an exceptionally high $^{87}Sr/^{86}Sr$ ratio (0.7061), which suggests that the vent may be over the Precambrian CLM, represented by the 0.706 line (Kistler, 1990; Beard and Glazner, 1995). Between 17 and 2 Ma, the combination of arc and extensional processes resulted in magma production from similar sources, all with a subduction trace-element signature. Only extension-related lavas younger than 2 Ma in age from western Nevada include a component of magma derived from non-subduction modified asthenosphere (Cousens et al., 2012).

SUMMARY

The mafic volcanic rocks from this study were geographically divided into three broad regions: central GB (age range 35–5 Ma) and eastern and western ACA (age range 16–2.5 Ma). Aside from a small subset of western ACA lavas, the eastern and western ACA lavas largely overlap in age and elemental and isotopic composition. Basalt and basaltic andesite lavas follow olivine-clinopyroxene + plagioclase fractionating phases, with clinopyroxene noted as the dominant phase. The effects of plagioclase fractionation are minimal for all mafic lavas, though greater in the GB mafic lavas compared to ACA lavas.

Most mafic melts are dominated by a lithospheric mantle component that is revealed in normalized incompatible element patterns and in Sr and Nd isotopic compositions. Lavas from a subsection of western ACA lavas, referred to as the westernmost ACA, are recognized by their lower $^{87}Sr/^{86}Sr$ values compared to lavas with equal $^{144}Nd/^{143}Nd$ values, possibly because the lavas are partial melts of less enriched lithospheric mantle compared to the CLM to the east. Trace-element data show that compositions of all mafic melts possess a subduction zone signature. This subduction signature, which includes negative Ta, Nb, and Ti anomalies and LREE + LILE enrichment, is weakest in the GB (older) mafic lavas where the dip angle

and dehydration from the slab was the lowest. The subduction signature is strongest in the western ACA (younger) mafic lavas, when the dip angle and slab dehydration into the mantle wedge was comparatively greater. The GB mafic lavas have likely obtained a subduction signature via melting of the metasomatized lithospheric mantle (i.e., the CLM was modified from exchange of incompatible elements from the slab during flat-slab subduction). While the Farallon slab rolled back across the GB, the shallow dip did not allow for large degrees of fluid release. For the ACA lavas, the slab dip was sufficient for fluid release into the mantle wedge, and thus, melting occurred in both the mantle wedge and the CLM. Increased fluids into the mantle wedge also produced higher volumes of melt, which explains the larger volumes of melt in the ACA compared to the GB.

Geochemical indicators that signify contributions from sediment melts (e.g., higher Th/Nb, Pb/Ce, and lower Ce/Ce*) are present for magmas west of longitude 120° (western and westernmost ACA lavas). The $^{207}Pb/^{204}Pb$ and $^{208}Pb/^{204}Pb$ values for the western ACA lavas are higher compared to the GB lavas at a given $^{143}Nd/^{144}Nd$ value but show no evidence of crustal contamination. It is therefore likely that the more radiogenic Pb was sourced from melted sediment rather than the crust.

Mafic lavas from the GB and selected eastern ACA lavas have higher K_2O, TiO_2, P_2O_5, HREE, and Nb contents for equal silica and lower Mg# values compared to the rest of the ACA lavas. These results are consistent with low degrees of partial melting due to (1) lower temperatures and water (volatile) abundances generated from the shallow slab for the GB mafic lavas and (2) faulting due to extension. Basaltic trachyandesites are more alkaline with higher $^{87}Sr/^{86}Sr$, suggesting these melts resulted from lower degrees of partially melted CLM. Great Basin extension at ca. 17–14 Ma in the Pyramid Lake region and Stillwater Range triggered lower-*F* melting that resulted in overall enrichment in incompatible elements but no change in incompatible element patterns. In this region, extension primarily causes melting of the CLM until ca. 2 Ma, when melting of the asthenosphere is first recorded in alkaline lavas from the Reno-Fallon corridor.

ACKNOWLEDGMENTS

This project was financially supported by Natural Sciences and Engineering Research Council (NSERC) grants to Dr. Brian Cousens with additional funding from the Mineralogical Association of Canada. Thank you especially to Dr. Christopher Henry and colleagues from the Nevada Bureau of Mines and Geology. Dr. Henry's expertise in the region and enthusiasm in the field have been extremely valuable and vital to the success of this project. I have benefited from the discussions and encouragement from the Cousens Community, including Dr. Richard Ernst, Christopher Rogers, Susan Kingdon, Alana MacKinder, Cole Kingsbury, and Seamus Magnus as a wonderfully encouraging group for scientific discussion and learning. Thanks also to Keith Bell, Lizzy Ann Spencer, Mike Jackson, Beth Halfkenny, John Blenkinsop, Claire Samson, and Sharon Carr for training, encouragement, and overwhelming support. Alan Donaldson, Ron Pickerill, Cliff Shaw, and David Lentz provided valuable reviews, support, and counsel. Finally, I am immensely honored and grateful for the time and valuable counsel from Geosphere editors, associate editors, and reviewers: Dr. Shanaka de Silva, Dr. Eric Christiansen, Dr. Keith Putirka, and Dr. Richard Bradshaw.

REFERENCES CITED

Arcay, D., Tric, E., and Doin, M.P., 2007, Slab surface temperature in subduction zones: Influence of the interplate decoupling depth and upper plate thinning processes: Earth and Planetary Science Letters, v. 255, no. 3, p. 324–338, https://doi.org/10.1016/j.epsl.2006.12.027.

Ashley, R.P., Goetz, A.F.H., Rowan, L.C., and Abrams, M.J., 1979, Detection and mapping of hydrothermally altered rocks in the vicinity of the Comstock Lode, Virginia Range, Nevada, using enhanced Landsat images: U.S. Geological Survey Open-File Report, 79-960, 41 p., https://doi.org/10.3133/ofr79960.

Asmerom, Y., Jacobsen, S.B., and Wernicke, B.P., 1994, Variations in magma source regions during large-scale continental extension, Death Valley region, western United States: Earth and Planetary Science Letters, v. 125, no. 1, p. 235–254, https://doi.org/10.1016/0012-821X(94)90218-6.

Atwater, T., and Stock, J., 1998, Pacific-North America plate tectonics of the Neogene southwestern United States: An update: International Geology Review, v. 40, no. 5, p. 375–402, https://doi.org/10.1080/00206819809465216.

Bacon, C.R., Bruggman, P.E., Christiansen, R.L., Clynne, M.A., Donnelly-Nolan, J.M., and Hildreth, W., 1997, Primitive magmas at five Cascades volcanic fields: Melts from hot, heterogeneous sub-arc mantle: Canadian Mineralogist, v. 35, p. 397–424.

Baker, M.B., Grove, T.L., and Price, R., 1994, Primitive basalts and andesites from the Mt. Shasta region, N. California: Products of varying melt fraction and water content: Contributions to Mineralogy and Petrology, v. 118, no. 2, p. 111–129, https://doi.org/10.1007/BF01052863.

Barbarin, B., Dodge, F.C.W., Kistler, R.W., and Bateman, P.C., 1989, Mafic inclusions, aggregates, and dikes in granitoid rocks, central Sierra Nevada batholith, California: U.S Geological Survey Bulletin 1899, 27 p., https://doi.org/10.3133/b1899.

Beard, B.L., and Glazner, A.F., 1995, Trace element and Sr and Nd isotopic composition of mantle xenoliths from the Big Pine volcanic field, California: Journal of Geophysical Research. Solid Earth, v. 100, p. 4169–4179, https://doi.org/10.1029/94JB02883.

Bell, J.W., and Bonham, Jr., H.F., 1987, Geologic map of the Vista Quadrangle, Nevada: Nevada Bureau of Mines and Geology Map, 1:24,000 scale.

Bell, J.W., and House, P.K., 2010, Geologic Map of the Grimes Point Quadrangle, Churchill County, Nevada: Nevada Bureau of Mines and Geology, 1 plate, 24 p., 1:24,000 scale.

Best, M.G., and Christiansen, E.H., 1991, Limited extension during peak Tertiary volcanism, Great Basin of Nevada and Utah: Journal of Geophysical Research. Solid Earth, v. 96, p. 13,509–13,528, https://doi.org/10.1029/91JB00244.

Best, M.G., Barr, D.L., Christiansen, E.H., Gromme, S., Deino, A.L., and Tingey, D.G., 2009, The Great Basin Altiplano during the middle Cenozoic ignimbrite flareup: Insights from volcanic rocks: International Geology Review, v. 51, no. 7–8, p. 589–633, https://doi.org/10.1080/00206810902867690.

Best, M.G., Christiansen, E.H., and Gromme, S., 2013, Introduction: The 36–18 Ma southern Great Basin, USA, ignimbrite province and flareup: Swarms of subduction-related supervolcanoes: Geosphere, v. 9, p. 260–274, https://doi.org/10.1130/GES00870.1.

Best, M.G., Christiansen, E.H., de Silva, S., and Lipman, P.W., 2016, Slab-rollback ignimbrite flareups in the southern Great Basin and other Cenozoic American arcs: A distinct style of arc volcanism: Geosphere, v. 12, p. 1097–1135, https://doi.org/10.1130/GES01285.1.

Bonham, H.F., and Papke, K.G., 1969, Geology and mineral deposits of Washoe and Storey Counties, Nevada, Mackay School of Mines, University of Nevada, v. 70.

Borg, L.E., 1989, Petrogenesis of Magee composite volcano, northern California [M.S. thesis]: University of Texas at Austin, 128 p.

Borg, L.E., Clynne, M.A., and Bullen, T.D., 1997, The variable role of slab-derived fluids in the generation of a suite of primitive calc-alkaline lavas from the southernmost Cascades, California: Canadian Mineralogist, v. 35, p. 425–452.

Borg, L.E., Blichert-Toft, J., and Clynne, M.A., 2002, Ancient and modern subduction zone contributions to the mantle sources of lavas from the Lassen region of California inferred from Lu-Hf isotopic systematics: Journal of Petrology, v. 43, no. 4, p. 705–723, https://doi.org/10.1093/petrology/43.4.705.

Boyd, O.S., Jones, C.H., and Sheehan, A.F., 2004, Foundering lithosphere imaged beneath the southern Sierra Nevada, California, USA: Science, v. 305, no. 5684, p. 660–662, https://doi.org/10.1126/science.1099181.

Briqueu, L., Bougault, H., and Joron, J.L., 1984, Quantification of Nb, Ta, Ti and V anomalies in magmas associated with subduction zones: Petrogenetic implications: Earth and Planetary Science Letters, v. 68, p. 297–308, https://doi.org/10.1016/0012-821X(84)90161-4.

Brown, R.J., Civetta, L., Arienzo, I., D'Antonio, M., Moretti, R., Orsi, G., Tomlinson, E.L., Albert, P.G., and Menzies, M.A., 2014, Geochemical and isotopic insights into the assembly, evolution and disruption of a magmatic plumbing system before and after a cataclysmic caldera-collapse eruption at Ischia volcano (Italy): Contributions to Mineralogy and Petrology, v. 168, p. 1035, https://doi.org/10.1007/s00410-014-1035-1.

Busby, C.J., 2012, Extensional and transtensional continental arc basins: Case studies from the southwestern United States, *in* Busby, C., and Azor, A., eds., Tectonics of Sedimentary Basins: Recent Advances: Wiley-Blackwell, p. 382–404, https://doi.org/10.1002/9781444347166.ch19.

Busby, C.J., 2013, Birth of a plate boundary at ca. 12 Ma in the Ancestral Cascades arc, Walker Lane belt of California and Nevada: Geosphere, v. 9, no. 5, p. 1147–1160, https://doi.org/10.1130/GES00928.1.

Busby, C.J., and Putirka, K., 2009, Miocene evolution of the western edge of the Nevadaplano in the central and northern Sierra Nevada: Palaeocanyons, magmatism, and structure: International Geology Review, v. 51, no. 7–8, p. 670–701, https://doi.org/10.1080/00206810902978265.

Busby, C.J., Hagan, J., Putirka, K., Pluhar, C., Gans, P., Wagner, D., Rood, D., DeOreo, S., and Skilling, I., 2008, The Ancestral Cascades arc: Cenozoic evolution of the central Sierra Nevada (California) and the birth of the new plate boundary, *in* Wright, J.E., and Shervais, J.W., eds., Ophiolites, Arcs and Batholiths: A Tribute to Cliff Hopson: Geological Society of America Special Paper 438, p. 331–378, https://doi.org/10.1130/2008.2438(12).

Camp, V.E., 1995, Mid-Miocene propagation of the Yellowstone mantle plume head beneath the Columbia River basalt source region: Geology, v. 23, no. 5, p. 435–438, https://doi.org/10.1130/0091-7613(1995)023<0435:MMPOTY>2.3.CO;2.

Castor, S.B., House, P.K. and Hudson, D.M., 2006, Preliminary geologic map of the Flowery Peak quadrangle, Storey and Lyon counties, Nevada: Nevada Bureau of Mines and Geology Open-File Report 06-16, scale 1:24,000.

Christiansen, R.L., Yeats, R.S., Graham, S.A., Niem, W.A., Niem, A.R., and Snavely, P.D., Jr., 1992, Post-Laramide geology of the US Cordilleran region, *in* Burchfiel, B.C., Lipman, P. W., and Zoback, M.L., eds., The Cordilleran Orogen: Conterminous U.S.: Boulder, Colorado, Geological Society of America, The Geology of North America, v. G-3 The Geology of North America, v. 3, p. 261–406.

Christiansen, R.L., Foulger, G.R., and Evans, J.R., 2002, Upper-mantle origin of the Yellowstone hotspot: Geological Society of America Bulletin, v. 114, no. 10, p. 1245–1256, https://doi.org/10.1130/0016-7606(2002)114<1245:UMOOTY>2.0.CO;2.

Church, S.E., 1976, The Cascade Mountains revisited: A re-evaluation in light of new lead isotopic data: Earth and Planetary Science Letters, v. 29, p. 175–188, https://doi.org/10.1016/0012-821X(76)90037-6.

Church, S.E., and Tilton, G.R., 1973, Lead and strontium isotopic studies in the Cascade Mountains: bearing on andesite genesis: Geological Society of America Bulletin, v. 84, p. 431–454, https://doi.org/10.1130/0016-7606(1973)84%3C431:LASISI%3E2.0.CO;2.

Class, C., and le Roex, A.P., 2008, Ce anomalies in Gough Island lavas—Trace element characteristics of a recycled sediment component: Earth and Planetary Science Letters, v. 265, no. 3, p. 475–486, https://doi.org/10.1016/j.epsl.2007.10.030.

Cline, J.S., Hofstra, A.H., Muntean, J.L., Tosdal, R.M., and Hickey, K.A., 2005, Carlin-type gold deposits in Nevada: Critical geologic characteristics and viable models: Economic Geology 100th anniversary volume, p. 451–484.

Cole, R.B., and Basu, A.R., 1995, Nd-Sr isotopic geochemistry and tectonics of ridge subduction and middle Cenozoic volcanism in western California: Geological Society of America Bulletin, v. 107, no. 2, p. 167–179, https://doi.org/10.1130/0016-7606(1995)107<0167:NSIGAT>2.3.CO;2.

Colgan, J.P., Dumitru, T.A., McWilliams, M., and Miller, E.L., 2006a, Timing of Cenozoic volcanism and Basin and Range extension in northwest Nevada: New constraints from the northern Pine Forest Ridge: Geological Society of America Bulletin, v. 118, p. 126–139, https://doi.org/10.1130/B25681.1.

Colgan, J.P., Dumitru, T.A., Reiners, P.W., Wooden, J.L., and Miller, E.L., 2006b, Cenozoic tectonic evolution of the Basin and Range province in northwestern Nevada: American Journal of Science, v. 306, p. 616–654, https://doi.org/10.2475/08.2006.02.

Coney, P.J., 1978, The plate tectonic setting of southeastern Arizona, *in* Callender, J.F, Wilt, J., Clemons, R.E., and James, H.L., eds., Land of Cochise (Southeastern Arizona): New Mexico Geological Society, 29th Annual Fall Field Conference Guidebook, p. 285–290.

Coney, P.J., and Reynolds, S.J., 1977, Cordilleran Benioff zones: Nature, v. 270, p. 403–406, https://doi.org/10.1038/270403a0.

Cousens, B., Prytulak, J., Henry, C., Alcazar, A., and Brownrigg, T., 2008, Geology, geochronology, and geochemistry of the Miocene–Pliocene Ancestral Cascades arc, northern Sierra Nevada, California and Nevada: The roles of the upper mantle, subducting slab, and the Sierra Nevada lithosphere: Geosphere, v. 4, no. 5, p. 829–853, https://doi.org/10.1130/GES00166.1.

Cousens, B., Henry, C.D., Timmermans, A., Sylvester, A., Wise, W., Prytulak, J., and Gupta, V., 2009, Miocene through Holocene arc and post-arc volcanism in the northern Sierra Nevada and western Nevada: American Geophysical Union Fall Meeting Abstracts, p. 2174

Cousens, B.L., 1996, Magmatic evolution of Quaternary mafic magmas at Long Valley Caldera and the Devils Postpile, California: Effects of crustal contamination on lithospheric mantle-derived magmas. Journal of Geophysical Research: Solid Earth, v. 101, no. B12, p. 27,673–27,689.

Cousens, B.L., Henry, C.D., Harvey, B.J., Brownrigg, T., Prytulak, J., and Allan, J.F., 2011, Secular variations in magmatism during a continental arc to post-arc transition: Plio-Pleistocene volcanism in the Lake Tahoe/Truckee area, Northern Sierra Nevada, California: Lithos, v. 123, no. 1, p. 225–242.

Cousens, B., Henry, C.D., and Gupta, V., 2012, Distinct mantle sources for Pliocene–Quaternary volcanism beneath the modern Sierra Nevada and adjacent Great Basin, northern California and western Nevada, USA: Geosphere, v. 8, no. 3, p. 562–580, https://doi.org/10.1130/GES00741.1.

Cousens, B., Wetmore, S., and Henry, C.D., 2013, The Pliocene–Quaternary Buffalo Valley volcanic field, Nevada: Post-extension, intraplate magmatism in the north-central Great Basin, USA: Journal of Volcanology and Geothermal Research, v. 268, p. 17–35, https://doi.org/10.1016/j.jvolgeores.2013.10.006.

Davis, A.S., and Clague, D.A., 1987, Geochemistry, mineralogy, and petrogenesis of basalt from the Gorda Ridge: Journal of Geophysical Research. Solid Earth, v. 92, p. 10467–10483, https://doi.org/10.1029/JB092iB10p10467.

Davis, A.S., Gunn, S.H., Bohrson, W.A., Gray, L.B., and Hein, J.R., 1995, Chemically diverse, sporadic volcanism at seamounts offshore southern and Baja California: Geological Society of America Bulletin, v. 107, p. 554–570, https://doi.org/10.1130/0016-7606(1995)107<0554:CDSVAS>2.3.CO;2.

Davis, A.S., Clague, D.A., and White, W.M., 1998, Geochemistry of basalt from Escanaba Trough: Evidence for sediment contamination?: Journal of Petrology, v. 39, p. 841–858, https://doi.org/10.1093/petrology/39.5.841.

DeCelles, P.G., 2004, Late Jurassic to Eocene evolution of the Cordilleran thrust belt and foreland basin system, western USA: American Journal of Science, v. 304, no. 2, p. 105–168, https://doi.org/10.2475/ajs.304.2.105.

Dickinson, W.R., 1997, Overview: Tectonic implications of Cenozoic volcanism in coastal California: Geological Society of America Bulletin, v. 109, p. 936–954, https://doig.org/10.1130/0016-7606(1997)109<0936:OTIOCV>2.3.CO;2.

Dickinson, W.R., 2002, The Basin and Range Province as a composite extensional domain: International Geology Review, v. 44, no. 1, p. 1–38, https://doi.org/10.2747/0020-6814.44.1.1.

Dickinson, W.R., 2004, Evolution of the North American cordillera: Annual Review of Earth and Planetary Sciences, v. 32, p. 13–45, https://doi.org/10.1146/annurev.earth.32.101802.120257.

Dickinson, W.R., 2006, Geotectonic evolution of the Great Basin: Geosphere, v. 2, no. 7, p. 353–368, https://doi.org/10.1130/GES00054.1.

Dickinson, W.R., 2013, Phanerozoic palinspastic reconstructions of Great Basin geotectonics (Nevada-Utah, USA): Geosphere, v. 9, p. 1384–1396, https://doi.org/10.1130/GES00888.1.

Dickinson, W.R., and Snyder, W.S., 1978, Plate tectonics of the Laramide orogeny: Geological Society of America, v. 151, p. 355–366, https://doi.org/10.1130/MEM151-p355.

du Bray, E.A., John, D.A., Putirka, K., and Cousens, B.L., 2009, Geochemical database for igneous rocks of the ancestral Cascades arc—Southern segment. California and Nevada: U.S. Geological Survey Digital Data Series, v. 439, no. 1.

Ducea, M., 2001, The California arc: Thick granitic batholiths, eclogitic residues, lithospheric-scale thrusting, and magmatic flare-ups: GSA Today, v. 11, no. 11, p. 4–10, https://doi.org/10.1130/1052-5173(2001)011<0004:TCATGB>2.0.CO;2.

Ducea, M., and Saleeby, J., 1998, A case for delamination of the deep batholithic crust beneath the Sierra Nevada, California: International Geology Review, v. 40, no. 1, p. 78–93, https://doi.org/10.1080/00206819809465199.

Ducea, M.N., and Saleeby, J.B., 1996, Buoyancy sources for a large, unrooted mountain range, the Sierra Nevada, California: Evidence from xenolith thermobarometry: Journal of Geophysical Research. Solid Earth, v. 101, no. B4, p. 8229–8244, https://doi.org/10.1029/95JB03452.

Dumitru, T.A., 1991, Effects of subduction parameters on geothermal gradients in forearcs, with an application to Franciscan Subduction in California: Journal of Geophysical Research, v. 96, no. B1, p. 621–641, https://doi.org/10.1029/90JB01913.

Elison, M.W., Speed, R.C., and Kistler, R.W., 1990, Geologic and isotopic constraints on the crustal structure of the northern Great Basin: Geological Society of America Bulletin, v. 102, no. 8, p. 1077–1092, https://doi.org/10.1130/0016-7606(1990)102<1077:GAICOT>2.3.CO;2.

Ellam, R.M., and Hawkesworth, C.J., 1988, Elemental and isotopic variations in subduction related basalts: Evidence for a three component model: Contributions to Mineralogy and Petrology, v. 98, no. 1, p. 72–80, https://doi.org/10.1007/BF00371911.

Elliott, T., 2003, Tracers of the slab, *in* Eiler, J., ed., Inside the Subduction Factory: American Geophysical Union Geophysical Monograph 138, p. 23–45, https://doi.org/10.1029/138GM03.

Elliott, T., Plank, T., Zindler A., White W., and Bourdon, B., 1997, Element transport from slab to volcanic front at the Mariana arc: Journal of Geophysical Research, v. 102, p. 14,991–15,019.

Elston, W.E., 1984, Subduction of young oceanic lithosphere and extensional orogeny in southwestern North America during Mid-Tertiary time: Tectonics, v. 3, no. 2, p. 229–250, https://doi.org/10.1029/TC003i002p00229.

English, J.M., and Johnston, S.T., 2004, The Laramide orogeny: What were the driving forces?: International Geology Review, v. 46, no. 9, p. 833–838, https://doi.org/10.2747/0020-6814.46.9.833.

English, J.M., Johnston, S.T., and Wang, K., 2003, Thermal modelling of the Laramide orogeny: Testing the flat-slab subduction hypothesis: Earth and Planetary Science Letters, v. 214, no. 3, p. 619–632, https://doi.org/10.1016/S0012-821X(03)00399-6.

Farmer, G.L., and DePaolo, D.J., 1983, Origin of Mesozoic and Tertiary granite in the western United States and implications for Pre-Mesozoic crustal structure: 1. Nd and Sr isotopic studies in the geocline of the Northern Great Basin: Journal of Geophysical Research. Solid Earth, v. 88, no. B4, p. 3379–3401, https://doi.org/10.1029/JB088iB04p03379.

Farmer, G.L., and DePaolo, D.J., 1984, Origin of Mesozoic and Tertiary granite in the western United States and implications for Pre-Mesozoic crustal structure: 2. Nd and Sr isotopic studies of unmineralized and Cu-and Mo-mineralized granite in the Precambrian Craton: Journal of Geophysical Research: Solid Earth, v. 89, p. 10,141–10,160.

Farmer, G.L., Glazner, A.F., Wilshire, H.G., Wooden, J.L., Pickthorn, W.J., and Katz, M., 1995, Origin of late Cenozoic basalts at the Cima volcanic field, Mojave Desert, California: Journal of Geophysical Research. Solid Earth, v. 100, no. B5, p. 8399–8415, https://doi.org/10.1029/95JB00070.

Farmer, G.L., Glazner, A.F., and Manley, C.R., 2002, Did lithospheric delamination trigger late Cenozoic potassic volcanism in the southern Sierra Nevada, California?: Geological Society of America Bulletin, v. 114, no. 6, p. 754–768, https://doi.org/10.1130/0016-7606(2002)114<0754:DLDTLC>2.0.CO;2.

Faulds, J.E., Henry, C.D., and Hinz, N.H., 2005, Kinematics of the northern Walker Lane: An incipient transform fault along the Pacific–North American plate boundary: Geology, v. 33, no. 6, p. 505–508, https://doi.org/10.1130/G21274.1.

Fitton, J.G., James, D., Kempton, P.D., Ormerod, D.S., and Leeman, W.P., 1988, The role of lithospheric mantle in the generation of late Cenozoic basic magmas in the western United States: Journal of Petrology, Special Volume, no. 1, p. 331–349, https://doi.org/10.1093/petrology/Special_Volume.1.331.

George, R., Turner, S., Hawkesworth, C., Morris, J., Nye, C., Ryan, J., and Zheng, S.H., 2003, Melting processes and fluid and sediment transport rates along the Alaska-Aleutian arc from an integrated U-Th-Ra-Be isotope study: Journal of Geophysical Research. Solid Earth, v. 108, https://doi.org/10.1029/2002JB001916.

GEOROC, 2007, Geochemistry of Rocks of the Oceans and Continents: Mainz, Max-Planck-Institute für Chemie, http://georoc.mpch-mainz.gwdg.de/georoc/ (last accessed March 2014).

Gill, J.B., 1981, Orogenic Andesites and Plate Tectonics: New York, Springer-Verlag, 390 p.

Glazner, A.F., Farmer, G.L., Hughes, W.T., Wooden, J., and Pickthorn, W., 1991, Contamination of basaltic magma by mafic crust at Amboy and Pisgah Craters, Mojave Desert, California: Journal of Geophysical Research. Solid Earth, v. 96, no. B8, p. 13,673–13,691, https://doi.org/10.1029/91JB00175.

Goldstein, S.L., and O'Nions, R.K., 1981, Nd and Sr isotopic relationships in pelagic clays and ferromanganese deposits: Nature, v. 292, p. 324–327, https://doi.org/10.1038/292324a0.

Green, D.H., and Hibberson, W., 1970, The instability of plagioclase in peridotite at high pressure: Lithos, v. 3, no. 3, p. 209–221, https://doi.org/10.1016/0024-4937(70)90074-5.

Green, D.H., Hibberson, W.O., Kovács, I., and Rosenthal, A., 2010, Water and its influence on the lithosphere-asthenosphere boundary: Nature, v. 467, no. 7314, p. 448–451, https://doi.org/10.1038/nature09369.

Green, N.L., and Harry, D.L., 1999, On the relationship between subducted slab age and arc basalt petrogenesis, Cascadia subduction system, North America: Earth and Planetary Science Letters, v. 171, no. 3, p. 367–381, https://doi.org/10.1016/S0012-821X(99)00159-4.

Green, N.L., and Sinha, A.K., 2005, Consequences of varied slab age and thermal structure on enrichment processes in the sub-arc mantle of the northern Cascadia subduction system: Journal of Volcanology and Geothermal Research, v. 140, no. 1, p. 107–132, https://doi.org/10.1016/j.jvolgeores.2004.07.017.

Gutscher, M.A., Maury, R., Eissen, J.P., and Bourdon, E., 2000a, Can slab melting be caused by flat subduction?: Geology, v. 28, no. 6, p. 535–538, https://doi.org/10.1130/0091-7613(2000)28<535:CSMBCB>2.0.CO;2.

Gutscher, M.A., Spakman, W., Bijwaard, H., and Engdahl, E.R., 2000b, Geodynamics of flat subduction: Seismicity and tomographic constraints from the Andean margin: Tectonics, v. 19, no. 5, p. 814–833, https://doi.org/10.1029/1999TC001152.

Hagan, J.C., Busby, C.J., Putirka, K., and Renne, P.R., 2009, Cenozoic palaeocanyon evolution, Ancestral Cascades arc volcanism, and structure of the Hope Valley–Carson Pass region, Sierra Nevada, California: International Geology Review, v. 51, no. 9–11, p. 777–823, https://doi.org/10.1080/00206810903028102.

Harker, A., 1909, The Natural History of Igneous Rocks: New York, Macmillan, 384 p.

Harry, D.L., and Green, N.L., 1999, Slab dehydration and basalt petrogenesis in subduction systems involving very young oceanic lithosphere: Chemical Geology, v. 160, no. 4, p. 309–333, https://doi.org/10.1016/S0009-2541(99)00105-9.

Hart, S.R., 1984, A large-scale isotope anomaly in the Southern Hemisphere mantle: Nature, v. 309, p. 753–757, https://doi.org/10.1038/309753a0.

Harwood, D.S., 1981, Geology of the Granite Chief Wilderness Study Area, California: U.S. Geological Survey Miscellaneous Field Studies Map MF-1273-A, scale 1:62,500.

Hawkesworth, C., Turner, S., Peate, D., McDermott, F., and van Calsteren, P., 1997, Elemental U and Th variations in island arc rocks: implications for U-series isotopes: Chemical Geology, v. 139, no. 1, p. 207–221, https://doi.org/10.1016/S0009-2541(97)00036-3.

Henry, C.D., 1996, Geologic map of the Bell Canyon quadrangle, western Nevada: Nevada Bureau of Mines and Geology, 14 p., scale 1:24,000.

Henry, C.D., 2008, Ash-flow tuffs and paleovalleys in northeastern Nevada: Implications for Eocene paleogeography and extension in the Sevier hinterland, northern Great Basin: Geosphere, v. 4, no. 1, p. 1–35, https://doi.org/10.1130/GES00122.1.

Henry, C.D., 2009, Uplift of the Sierra Nevada, California: Geology, v. 37, p. 575–576, https://doi.org/10.1130/focus062009.1.

Henry, C.D., and John, D.A., 2013, Magmatism, ash-flow tuffs, and calderas of the ignimbrite flareup in the western Nevada volcanic field, Great Basin, USA: Geosphere, v. 9, no. 4, p. 951–1008, https://doi.org/10.1130/GES00867.1.

Henry, C.D., and Perkins, M.E., 2001, Sierra Nevada–Basin and Range transition near Reno, Nevada: Two-stage development at 12 and 3 Ma: Geology, v. 29, no. 8, p. 719–722.

Henry, C.D., and Ressel, M.W., 2000, Eocene magmatism of northeastern Nevada: The smoking gun for Carlin-type gold deposits, *in* Cluer, J.K., Price, J.G., Struhsacker, E.M., Hardyman, R.F., and Morris, C.L., eds., Geology and Ore Deposits 2000: The Great Basin and Beyond. Geological Society of Nevada Symposium Proceedings: Reno, Nevada, 15–18 May 2000, p. 365–388.

Henry, C.D., and Sloan, J., 2003, Isotopic age database for the Great Basin and adjacent regions, Nevada Bureau of Mines and Geology: http://mapserver.library.unr.edu/website/dataworksweb/NevadaRocks/viewer.htm.

Henry, C.D., Castor, S.B., and Elson, H.B., 1996, Geology and $^{40}Ar/^{39}Ar$ geochronology of volcanism and mineralization at Round Mountain, Nevada, *in* Coyner, A.R., and Fahey, P.L., eds., Geology and Ore Deposits of the American Cordillera: Reno/Sparks, Symposium Proceedings, Geological Society of Nevada, p. 283–307.

Henry, C.D., Elson, H.B., McIntosh, W.C., Heizler, M.T., and Castor, S.B., 1997, Brief duration of hydrothermal activity at Round Mountain, Nevada, determined from $^{40}Ar/^{39}Ar$ geochronology: Economic Geology and the Bulletin of the Society of Economic Geologists, v. 92, no. 7–8, p. 807–826, https://doi.org/10.2113/gsecongeo.92.7-8.807.

Henry, C.D., Cousens, B.L., Castor, S.B., Faulds, J.E., Garside, L.J., and Timmermans, A., 2004b, The Ancestral Cascades Arc, northern California/western Nevada: Spatial and Temporal Variations in Volcanism and Geochemistry: AGU Fall Meeting Abstracts, v. 1, p. 1478.

Henry, C.D., Faulds, J.E., dePolo, C.M., and Davis, D.A., 2004a, Geology of the Dogskin Mountain quadrangle. Washoe County, Nevada: Nevada Bureau of Mines and Geology Map 148, 13 p.

Henry, C.D., Faulds, J.E., dePolo, C.M., and Davis, D.A., 2004c, Geologic map of the Dogskin Mountain Quadrangle. Washoe County, Nevada: Nevada Bureau of Mines and Geology Map 148, scale 1:24,000.

Henry, C.D., McGrew, A.J., Colgan, J.P., Snoke, A.W., and Brueseke, M.E., 2011, Timing, distribution, amount, and style of Cenozoic extension in the northern Great Basin, *in* Lee, J., and Evans, J.P., eds., Geologic Field Trips to the Basin and Range, Rocky Mountains, Snake River Plain, and Terranes of the U.S. Cordillera: Geological Society of America Field Guide 21, p. 27–66, https://doi.org/10.1130/2011.0021(02).

Hofmann, A.W., Feigenson, M.D., and Raczek, I., 1984, Case studies on the origin of basalt: III. Petrogenesis of the Mauna Ulu eruption, Kilauea, 1969–1971: Contributions to Mineralogy

and Petrology, v. 88, no. 1–2, p. 24–35, https://doi.org/10.1007/BF00371409.

Hofstra, A.H., Snee, L.W., Rye, R.O., Folger, H.W., Phinisey, J.D., Loranger, R.J., and Lewchuk, M.T., 1999, Age constraints on Jerritt Canyon and other Carlin-type gold deposits in the Western United States; relationship to mid-Tertiary extension and magmatism: Economic Geology and the Bulletin of the Society of Economic Geologists, v. 94, no. 6, p. 769–802, https://doi.org/10.2113/gsecongeo.94.6.769.

Hudson, F.S., 1951, Mount Lincoln-Castle Peak Area Sierra Nevada, California: Geological Society of America Bulletin, v. 62, no. 8, p. 931–952, https://doi.org/10.1130/0016-7606(1951)62[931:MLPASN]2.0.CO;2.

Hudson, D.M., Castor, S.B., Garside, L.J., and Henry, C.D., 2009, Geologic map of the Virginia City quadrangle, Washoe, Storey, and Lyon Counties and Carson City, Nevada: Nevada Bureau of Mines and Geology Map 165, 2 plates and text, scale 1:24,000.

Hudson, M.R., John, D.A., Conrad, J.E., and McKee, E.H., 2000, Style and age of late Oligocene–early Miocene deformation in the southern Stillwater Range, west central Nevada: Paleomagnetism, geochronology, and field relations: Journal of Geophysical Research. Solid Earth, v. 105, no. B1, p. 929–954, https://doi.org/10.1029/1999JB900338.

Hughes, S.S., 1990, Mafic magmatism and associated tectonism of the central High Cascade Range, Oregon: Journal of Geophysical Research. Solid Earth, v. 95, no. B12, p. 19,623–19,638, https://doi.org/10.1029/JB095iB12p19623.

Humphreys, E., Hessler, E., Dueker, K., Farmer, G.L., Erslev, E., and Atwater, T., 2003, How Laramide-age hydration of North American lithosphere by the Farallon slab controlled subsequent activity in the western United States: International Geology Review, v. 45, no. 7, p. 575–595, https://doi.org/10.2747/0020-6814.45.7.575.

Humphreys, E.D., 1995, Post-Laramide removal of the Farallon slab, western United States: Geology, v. 23, no. 11, p. 987–990, https://doi.org/10.1130/0091-7613(1995)023<0987:PLROTF>2.3.CO;2.

Irvine, T., and Baragar, W., 1971, A guide to the chemical classification of the common volcanic rocks: Canadian Journal of Earth Sciences, v. 8, no. 5, p. 523–548, https://doi.org/10.1139/e71-055.

John, D.A., 1995, Tilted middle Tertiary ash-flow calderas and subjacent granitic plutons, southern Stillwater Range, Nevada: Cross sections of an Oligocene igneous center: Geological Society of America Bulletin, v. 107, no. 2, p. 180–200, https://doi.org/10.1130/0016-7606(1995)107<0180:TMTAFC>2.3.CO;2.

John, D.A., 2001, Miocene and early Pliocene epithermal gold-silver deposits in the northern Great Basin, western United States: Characteristics, distribution, and relationship to magmatism: Economic Geology and the Bulletin of the Society of Economic Geologists, v. 96, no. 8, p. 1827–1853, https://doi.org/10.2113/gsecongeo.96.8.1827.

John, D.A., Henry, C.D., and Colgan, J.P., 2008, Magmatic and tectonic evolution of the Caetano caldera, north-central Nevada: A tilted, mid-Tertiary eruptive center and source of the Caetano Tuff: Geosphere, v. 4, no. 1, p. 75–106, https://doi.org/10.1130/GES00116.1.

John, D.A., du Bray, E.A., Blakely, R.J., Fleck, R.J., Vikre, P.G., Box, S.E., and Moring, B.C., 2012, Miocene magmatism in the Bodie Hills volcanic field, California and Nevada: A long-lived eruptive center in the southern segment of the ancestral Cascades arc: Geosphere, v. 8, p. 44–97, https://doi.org/10.1130/GES00674.1.

Johnson, M.C., and Plank, T., 1999, Dehydration and melting experiments constrain the fate of subducted sediments: Geochemistry, Geophysics, Geosystems, v. 1, https://doi.org/10.1029/1999GC000014.

Jones, A.E., 1997, Geologic map of the Hot Springs Peak quadrangle and the southeastern part of the Little Poverty quadrangle, Nevada: Nevada Bureau of Mines and Geology, 1:24,000 scale.

Jordan, B.T., Grunder, A.L., Duncan, R.A., and Deino, A.L., 2004, Geochronology of age-progressive volcanism of the Oregon High Lava Plains: Implications for the plume interpretation of Yellowstone: Journal of Geophysical Research. Solid Earth, v. 109, no. B10.

Kempton, P.D., Fitton, J.G., Hawkesworth, C.J., and Ormerod, D.S., 1991, Isotopic and trace element constraints on the composition and evolution of the lithosphere beneath the southwestern United States. Journal of Geophysical Research: Solid Earth, no. 1978–2012, v. 96, no. B8, p. 13,713–13,735.

Kent, G.M., Babcock, J.M., Driscoll, N.W., Harding, A.J., Dingler, J.A., Seitz, G.G., Gardner, J.V., Mayer, L.A., Goldman, C.R., Hayvaert, A.C., Richards, R.C., Karlin, R., Morgan, C.W., Gayes, P.T., and Owen, L.A., 2005, 60 k.y. record of extension across the western boundary of the Basin and Range province: Estimates of slip rates from offset shoreline terraces and a catastrophic slide beneath Lake Tahoe: Geology, v. 33, p. 365–368, https://doi.org/10.1130/G21230.1.

Kessel, R., Schmidt, M.W., Ulmer, P., and Pettke, T., 2005, Trace element signature of subduction-zone fluids, melts and supercritical liquids at 120–180 km depth: Nature, v. 437, p. 724, https://doi.org/10.1038/nature03971.

Kinzler, R.J., 1997, Melting of mantle peridotite at pressures approaching the spinel to garnet transition: Application to mid-ocean ridge basalt petrogenesis: Journal of Geophysical Research: Solid Earth, v. 102, p. 853–874, https://doi.org/10.1029/96JB00988.

Kistler, R.W., 1990, Two different lithosphere types in the Sierra Nevada, California: Geological Society of America, v. 174, p. 271–282, https://doi.org/10.1130/MEM174-p271.

Kistler, R.W., and Peterman, Z.E., 1973, Variations in Sr, Rb, K, Na, and initial Sr^{87}/Sr^{86} in Mesozoic granitic rocks and intruded wall rocks in central California: Geological Society of America Bulletin, v. 84, no. 11, p. 3489–3512, https://doi.org/10.1130/0016-7606(1973)84<3489:VISRKN>2.0.CO;2.

Kistler, R.W., and Peterman, Z.E., 1978, Reconstruction of crustal blocks of California on the basis of initial strontium isotopic compositions of Mesozoic granite rocks: U.S. Geological Survey Professional Paper 1071, 17 p.

Labanieh, S., Chauvel, C., Germa, A., and Quidelleur, X., 2012, Martinique: A clear case for sediment melting and slab dehydration as a function of distance to the trench: Journal of Petrology, v. 53, p. 2441–2464, https://doi.org/10.1093/petrology/egs055.

Lackschewitz, K.S., Singer, A., Botz, R., Garbe-Schönberg, D., and Stoffers, P., 2000, Mineralogy and geochemistry of clay minerals near a hydrothermal site in the Escanaba Trough, Gorda Ridge, northeast Pacific Ocean, *in* Zierenberg, R.A., Fouquet, Y., Miller, D.J., and Normark, W.R., eds., Proceedings of the Ocean Drilling Program, Scientific Results, v. 169, p. 1–24.

Latham, T.S., 1985, Stratigraphy, structure, and geochemistry of Plio-Pleistocene volcanic rocks of the western Basin and Range Province, near Truckee, California [Ph.D. dissertation]: University of California, Davis, 340 p.

Le Bas, M.J., Le Maitre, R.W., Streckeisen, A., and Zanettin, B., 1986, A chemical classification of volcanic rocks based on the total alkali-silica diagram: Journal of Petrology, v. 27, no. 3, p. 745–750, https://doi.org/10.1093/petrology/27.3.745.

Lee, C.T., Yin, Q., Rudnick, R.L., and Jacobsen, S.B., 2001, Preservation of ancient and fertile lithospheric mantle beneath the southwestern United States: Nature, v. 411, no. 6833, p. 69–73, https://doi.org/10.1038/35075048.

Lee, C.T.A., 2005, Trace element evidence for hydrous metasomatism at the base of the North American lithosphere and possible association with Laramide low-angle subduction: The Journal of Geology, v. 113, no. 6, p. 673–685, https://doi.org/10.1086/449327.

Leeman, W.P., Smith, D.R., Hildreth, W., Palacz, Z., and Rogers, N., 1990, Compositional diversity of late Cenozoic basalts in a transect across the southern Washington Cascades: Implications for subduction zone magmatism: Journal of Geophysical Research. Solid Earth, v. 95, no. B12, p. 19,561–19,582, https://doi.org/10.1029/JB095iB12p19561.

Leeman, W.P., Tonarini, S., Chan, L.H., and Borg, L.E., 2004, Boron and lithium isotopic variations in a hot subduction zone—The southern Washington Cascades: Chemical Geology, v. 212, no. 1, p. 101–124, https://doi.org/10.1016/j.chemgeo.2004.08.010.

Lipman, P.W., 1992, Magmatism in the Cordilleran United States: Progress and problems: The Geology of North America, v. 3, p. 481–514.

Lipman, P.W., Doe, B.R., Hedge, C.E., and Steven, T.A., 1978, Petrologic evolution of the San Juan volcanic field, southwestern Colorado: Pb and Sr isotope evidence: Geological Society of America Bulletin, v. 89, p. 59–82, https://doi.org/10.1130/0016-7606(1978)89<59:PEOTSJ>2.0.CO;2.

Liu, L., Spasojević, S., and Gurnis, M., 2008, Reconstructing Farallon plate subduction beneath North America back to the Late Cretaceous: Science, v. 322, p. 934–938, https://doi.org/10.1126/science.1162921.

Liu, L., Gurnis, M., Seton, M., Saleeby, J., Müller, R.D., and Jackson, J.M., 2010, The role of oceanic plateau subduction in the Laramide orogeny: Nature Geoscience, v. 3, no. 5, p. 353, https://doi.org/10.1038/ngeo829.

Manley, C.R., Glazner, A.F., and Farmer, G.L., 2000, Timing of volcanism in the Sierra Nevada of California: Evidence for Pliocene delamination of the batholithic root?: Geology, v. 28, no. 9, p. 811–814, https://doi.org/10.1130/0091-7613(2000)28<811:TOVITS>2.0.CO;2.

Mann, P., 2007, Overview of the tectonic history of northern Central America: Geological Society of America Special Papers, v. 428, p. 1–19, https://doi.org/10.1130/2007.2428(01).

McKenzie, D., 1989, Some remarks on the movement of small melt fractions in the mantle: Earth and Planetary Science Letters, v. 95, p. 53–72, https://doi.org/10.1016/0012-821X(89)90167-2.

Menzies, M.A., Leeman, W.P., and Hawkesworth, C.J., 1983, Isotope geochemistry of Cenozoic volcanic rocks reveals

mantle heterogeneity below western USA: Nature, v. 303, no. 5914, p. 205–209, https://doi.org/10.1038/303205a0.

Mitrovica, J.X., Beaumont, C., and Jarvis, G.T., 1989, Tilting of continental interiors by the dynamical effects of subduction: Tectonics, v. 8, no. 5, p. 1079–1094, https://doi.org/10.1029/TC008i005p01079.

Morrison, R.B., 1964, Lake Lahontan: Geology of southern Carson desert, Nevada: U.S. Geological Survey Professional Paper 401, 153 p.

Nichols, G.T., Wyllie, P.J., and Stern, C.R., 1994, Subduction zone melting of pelagic sediments constrained by melting experiments: Nature, v. 371, p. 785, https://doi.org/10.1038/371785a0.

Ormerod, D.S., 1988, Late- to post-subduction magmatic transitions in the western Great Basin, USA [Ph.D. thesis]: Milton Keynes, UK, The Open University, 313 p.

Ormerod, D.S., Hawkesworth, C.J., Rogers, N.W., Leeman, W.P., and Menzies, M.A., 1988, Tectonic and magmatic transitions in the Western Great Basin, USA: Nature, v. 333, no. 6171, p. 349–353, https://doi.org/10.1038/333349a0.

Ormerod, D.S., Rogers, N.W., and Hawkesworth, C.J., 1991, Melting in the lithospheric mantle: Inverse modeling of alkali-olivine basalts from the Big Pine Volcanic Field, California: Contributions to Mineralogy and Petrology, v. 108, no. 3, p. 305–317.

Page, B.M., 1965, Preliminary geologic map of a part of the Stillwater Range, Churchill County, Nevada: Nevada Bureau of Mines and Geology Map 28, scale 1:125,000.

Peacock, S.M., 1996, Thermal and petrologic structure of subduction zones: Subduction top to bottom, p. 119–133.

Peacock, S.M., Rushmer, T., and Thompson, A.B., 1994, Partial melting of subducting oceanic crust: Earth and Planetary Science Letters, v. 121, no. 1, p. 227–244, https://doi.org/10.1016/0012-821X(94)90042-6.

Pearce, J.A., 1983, Role of the sub-continental lithosphere in magma genesis at active continental margins, *in* Hawkesworth, C.J., and Norry, M.J., eds., Continental Basalts and Mantle Xenoliths: Nantwich, Cheshire: Shiva Publications, p. 230–249.

Pearce, J.A., 2008, Geochemical fingerprinting of oceanic basalts with applications to ophiolite classification and the search for Archean oceanic crust: Lithos, v. 100, no. 1, p. 14–48, https://doi.org/10.1016/j.lithos.2007.06.016.

Pearce, J.A., and Parkinson, I.J., 1993, Trace element models for mantle melting: Application to volcanic arc petrogenesis, *in* Prichard, H.M., Alabaster, T., Harris, N.B.W., and Neary, C.R., eds., Magmatic Processes and Plate Tectonics: Geological Society of London Special Publication 76, p. 373–403, https://doi.org/10.1144/GSL.SP.1993.076.01.19.

Pearce, J.A., and Peate, D.W., 1995, Tectonic implications of the composition of volcanic arc magmas: Annual Review of Earth and Planetary Sciences, v. 23, p. 251–285, https://doi.org/10.1146/annurev.ea.23.050195.001343.

Pearce, J.A., and Stern, R.J., 2006, Origin of back-arc basin magmas: Trace element and isotope perspectives. Back-Arc Spreading Systems: Geological, Biological, Chemical, and Physical Interactions, p. 63–86.

Perry, F.V., DePaolo, D.J., and Baldridge, W.S., 1993, Neodymium isotopic evidence for decreasing crustal contributions to Cenozoic ignimbrites of the western United States: Implications for the thermal evolution of the Cordilleran crust: Geological Society of America Bulletin, v. 105, no. 7, p. 872–882, https://doi.org/10.1130/0016-7606(1993)105<0872:NIEFDC>2.3.CO;2.

Plank, T., and Langmuir, C.H., 1988, An evaluation of the global variations in the major element chemistry of arc basalts: Earth and Planetary Science Letters, v. 90, p. 349–370, https://doi.org/10.1016/0012-821X(88)90135-5.

Plank, T., and Langmuir, C.H., 1992, Effects of the melting regime on the composition of the oceanic crust: Journal of Geophysical Research: Solid Earth, v. 97, p. 19,749–19,770, https://doi.org/10.1029/92JB01769.

Plank, T., and Langmuir, C.H., 1993, Tracing trace elements from sediment input to volcanic output at subduction zones: Nature, v. 362, p. 739.

Plank, T., and Langmuir, C.H., 1998, The chemical composition of subducting sediment and its consequences for the crust and mantle: Chemical Geology, v. 145, p. 325–394.

Priest, G.R., 1990, Volcanic and tectonic evolution of the Cascade volcanic arc, central Oregon: Journal of Geophysical Research. Solid Earth, v. 95, no. B12, p. 19,583–19,599, https://doi.org/10.1029/JB095iB12p19583.

Prytulak, J., Vervoort, J.D., Plank, T., and Yu, C., 2006, Astoria Fan sediments, DSDP site 174, Cascadia Basin: Hf-Nd-Pb constraints on provenance and outburst flooding: Chemical Geology, v. 233, no. 3, p. 276–292, https://doi.org/10.1016/j.chemgeo.2006.03.009.

Putirka, K., and Busby, C.J., 2007, The tectonic significance of high-K2O volcanism in the Sierra Nevada, California: Geology, v. 35, no. 10, p. 923–926, https://doi.org/10.1130/G23914A.1.

Putirka, K., Jean, M., Cousens, B., Sharma, R., Torrez, G., and Carlson, C., 2012, Cenozoic volcanism in the Sierra Nevada and Walker Lane, California, and a new model for lithosphere degradation: Geosphere, v. 8, no. 2, p. 265–291, https://doi.org/10.1130/GES00728.1.

Putirka, K.D., and Busby, C.J., 2011, Introduction: origin and evolution of the Sierra Nevada and Walker Lane: Geosphere, v. 7, no. 6, p. 1269–1272, https://doi.org/10.1130/GES00761.1.

Rasoazanamparany, C., Widom, E., Valentine, G.A., Smith, E.I., Cortes, J.A., Kuentz, D., and Johnsen, R., 2015, Origin of chemical and isotopic heterogeneity in a mafic, monogenetic volcanic field: A case study of the Lunar Crater Volcanic Field, Nevada: Chemical Geology, v. 397, p. 76–93, https://doi.org/10.1016/j.chemgeo.2015.01.004.

Reid, M.R., and Ramos, F.C., 1996, Chemical dynamics of enriched mantle in the southwestern United States: Thorium isotope evidence: Earth and Planetary Science Letters, v. 138, no. 1, p. 67–81, https://doi.org/10.1016/0012-821X(95)00234-4.

Ressel, M.W., and Henry, C.D., 2006, Igneous geology of the Carlin Trend, Nevada: development of the Eocene plutonic complex and significance for Carlin-type gold deposits: Economic Geology and the Bulletin of the Society of Economic Geologists, v. 101, no. 2, p. 347–383, https://doi.org/10.2113/gsecongeo.101.2.347.

Rollinson, H.R., 2014, Using Geochemical Data: Evaluation, Presentation, Interpretation: London, Routledge, 384 p., https://doi.org/10.4324/9781315845548.

Saleeby, J., 2003, Segmentation of the Laramide slab—Evidence from the southern Sierra Nevada region: Geological Society of America Bulletin, v. 115, no. 6, p. 655–668, https://doi.org/10.1130/0016-7606(2003)115<0655:SOTLSF>2.0.CO;2.

Saucedo, G.J., and Wagner, D.L., Compilers, 1992, Geologic map of the Chico Quadrangle: California Department of Conservation, Division of Mines and Geology, Regional Geologic Map Series Map 7A, 1:250,000.

Saucedo, G.J., Little, J.D., Watkins, S.E., Davis, J.R., Mascorro, M.T., Walker, V.D., and Ford, E.W., 2005, Geologic map of the Lake Tahoe basin, California and Nevada: California Geological Survey Regional Geologic Map no. 4, scale 1:100,000.

Schellart, W.P., Stegman, D.R., Farrington, R.J., Freeman, J., and Moresi, L., 2010, Cenozoic tectonics of western North America controlled by evolving width of Farallon slab: Science, v. 329, no. 5989, p. 316–319, https://doi.org/10.1126/science.1190366.

Seedorff, E., 1991, Magmatism, extension, and ore deposits of Eocene to Holocene age in the Great Basin—Mutual effects and preliminary proposed genetic relationships, *in* Raines, G.L., Lisle, R.E., Schafer, R.W., and Wilkinson, W.H., eds., Geology and Ore Deposits of the Great Basin: Reno, Geological Society of Nevada, v. 1, p. 133–178.

Sloan, J., Henry, C.D., Hopkins, M., and Ludington, S., 2003, Revision of national geochronological database: U.S. Geological Survey Open-File Report 03-236: http://wrgis.wr.usgs.gov/open-file/of03-236/.

Smith, D., Connelly, J.N., Manser, K., Moser, D.E., Housh, T.B., McDowell, F.W., and Mack, L.E., 2004, Evolution of Navajo eclogites and hydration of the mantle wedge below the Colorado Plateau, southwestern United States: Geochemistry, Geophysics, Geosystems, v. 5, https://doi.org/10.1029/2003GC000675.

Smith, E.I., Sanchez, A., Walker, J.D., and Wang, K., 1999, Geochemistry of mafic magmas in the Hurricane Volcanic field, Utah: Implications for small-and large-scale chemical variability of the lithospheric mantle: The Journal of Geology, v. 107, p. 433–448.

Sonder, L.J., and Jones, C.H., 1999, Western United States extension: How the west was widened: Annual Review of Earth and Planetary Sciences, v. 27, no. 1, p. 417–462, https://doi.org/10.1146/annurev.earth.27.1.417.

Spencer, J.E., Richard, S.M., Reynolds, S.J., Miller, R.J., Shafiqullah, M., Gilbert, W.G., and Grubensky, M.J., 1995, Spatial and temporal relationships between mid-Tertiary magmatism and extension in southwestern Arizona: Journal of Geophysical Research. Solid Earth, v. 100, no. B6, p. 10,321–10,351, https://doi.org/10.1029/94JB02817.

Stewart, J.H., 1999, Geologic map of the Carson City 30 × 60 minute quadrangle, Nevada: Nevada Bureau of Mines and Geology Map 118, 12 p.

Stewart, J.H., and Carlson, J.E., 1976, Cenozoic rocks of Nevada: Four maps and brief description of distribution, lithology, age, and centers of volcanism: Nevada Bureau of Mines and Geology, University of Nevada, Map 52, scale 1:1,000,000.

Strong, M., and Wolff, J., 2003, Compositional variations within scoria cones: Geology, v. 31, no. 2, p. 143–146, https://doi.org/10.1130/0091-7613(2003)031<0143:CVWSC>2.0.CO;2.

Sun, S.S., and McDonough, W.F., 1989, Chemical and isotopic systematics of oceanic basalts: implications for mantle composition and processes: Geological Society of London, Special Publications, v. 42, no. 1, p. 313–345, https://doi.org/10.1144/GSL.SP.1989.042.01.19.

Takada, A., 1994, The influence of regional stress and magmatic input on styles of monogenetic and polygenetic

volcanism: Journal of Geophysical Research. Solid Earth, v. 99, p. 13,563–13,573, https://doi.org/10.1029/94JB00494.
Thompson, G.A., and White, D.E., 1964, Regional geology of the Steamboat Springs area, Washoe County, Nevada: volcanic geology, structure, and mineral deposits of the Mount Rose quadrangle and additional data from the Virginia City and nearby quadrangles: U.S. Geological Survey Professional Paper 458-A, 52 p., https://doi.org/10.3133/pp458A.
Timmermans, A.C., 2015, A Geochemical Study of Cenozoic Magmatism along an East-West Transect from Central Great Basin, Nevada to the Ancestral Cascade Arc, California–A Compositional Journey over Space and Time [Doctoral dissertation]: Carleton University.
Todt, W., Cliff, R.A., Hanser, A., and Hofmann, A.W., 1996, Evaluation of a ^{202}Pb–^{205}Pb Double Spike for High-Precision Lead Isotope Analysis. Earth processes: Reading the isotopic code, p. 429–437.
Wakabayashi, J., 1992, Nappes, tectonics of oblique plate convergence, and metamorphic evolution related to 140 million years of continuous subduction, Franciscan Complex, California: The Journal of Geology, v. 100, p. 19–40, https://doi.org/10.1086/629569.
Weaver, C.S., Grant, W.C., and Shemeta, J.E., 1987, Local crustal extension at Mount St. Helens, Washington: Journal of Geophysical Research: Solid Earth, v. 92, p. 10,170–10,178, https://doi.org/10.1029/JB092iB10p10170.
Weber, M.E., and Smith, E.I., 1987, Structural and geochemical constraints on the reassembly of disrupted mid-Miocene volcanoes in the Lake Mead–Eldorado Valley area of southern Nevada: Geology, v. 15, no. 6, p. 553–556, https://doi.org/10.1130/0091-7613(1987)15<553:SAGCOT>2.0.CO;2.
Wernicke, B., and Snow, J.K., 1998, Cenozoic tectonism in the central Basin and Range: Motion of the Sierran-Great Valley block: International Geology Review, v. 40, no. 5, p. 403–410, https://doi.org/10.1080/00206819809465217.
Wernicke, B., Clayton, R., Ducea, M., Jones, C.H., Park, S., Ruppert, S., Saleeby, J., Snow, J.K., Squires, L., Fliedner, M., and Jiracek, G., 1996, Origin of high mountains in the continents: The southern Sierra Nevada: Science, v. 271, p. 190–193, https://doi.org/10.1126/science.271.5246.190.
White, W.M., 2013, Geochemistry: Chichester, UK, Wiley-Blackwell, 672 p.
Willden, R., and Speed, R.C., 1974, Geology and mineral deposits of Churchill County, Nevada, no. 83–85, Mackay School of Mines, University of Nevada, Reno.
Yogodzinski, G.M., Naumann, T.R., Smith, E.I., Bradshaw, T.K., and Walker, J.D., 1996, Evolution of a mafic volcanic field in the central Great Basin, south central Nevada: Journal of Geophysical Research. Solid Earth, v. 101, no. B8, p. 17,425–17,445, https://doi.org/10.1029/96JB00816.
Yusoff, Z.M., Ngwenya, B.T., and Parsons, I., 2013, Mobility and fractionation of REEs during deep weathering of geochemically contrasting granites in a tropical setting, Malaysia: Chemical Geology, v. 349, p. 71–86, https://doi.org/10.1016/j.chemgeo.2013.04.016.
Zandt, G., Gilbert, H., Owens, T.J., Ducea, M., Saleeby, J., and Jones, C.H., 2004, Active foundering of a continental arc root beneath the southern Sierra Nevada in California: Nature, v. 431, p. 41–46, https://doi.org/10.1038/nature02847.